Am J Cancer Res 2023;13(2):569-588
www.ajcr.us /ISSN:2156-6976/ajcr0147363

Original Article

Identification and validation of the cellular senescence-related molecular subtypes of triple negative breast cancer via integrating bulk and single-cell RNA sequencing data

Gaoda Ju[1*], Kai Zeng[2*], Linlin Lu[3*], Han Diao[4], Hao Wang[5], Xiaomin Li[6], Tianhao Zhou[7]

[1]Department of Medical Oncology, Key Laboratory of Carcinogenesis & Translational Research (Ministry of Education/Beijing), Peking University Cancer Hospital and Institute, Beijing 100142, China; [2]Department of Thyroid Surgery, The Eighth Affiliated Hospital, Sun Yat-sen University, Shenzhen 518000, Guangdong, China; [3]Department of Thyroid and Breast Surgery, The First Affiliated Hospital of Soochow University, Suzhou 215000, Jiangsu, China; [4]Department of Pathology, Affiliated Hospital of Jining Medical University, Jining 272000, Shandong, China; [5]Yancheng TCM Hospital, Nanjing University of Chinese Medicine, Yancheng 224002, Jiangsu, China; [6]Department of Radiology, Shanghai Ninth People's Hospital, Shanghai Jiao Tong University School of Medicine, Shanghai, China; [7]Department of Medical Oncology, Shanghai First People's Hospital, Shanghai Jiao Tong University School of Medicine, Shanghai 200080, China. [*]Equal contributors.

Received October 30, 2022; Accepted January 30, 2023; Epub February 15, 2023; Published February 28, 2023

Abstract: Patients with triple-negative breast cancer (TNBC) reportedly benefit from immune checkpoint blockade (ICB) therapy. However, the subtype-specific vulnerabilities of ICB in TNBC remain unclear. As the complex interplay between cellular senescence and anti-tumor immunity has been previously discussed, we aimed to identify markers related to cellular senescence that may serve as potential predictors of response to ICB in TNBC. We used three transcriptomic datasets derived from ICB-treated breast cancer samples at both scRNA-seq and bulk-RNA-seq levels to define the subtype-specific vulnerabilities of ICB in TNBC. Differences in the molecular features and immune cell infiltration among the different TNBC subtypes were further explored using two scRNA-seq, three bulk-RNA-seq, and two proteomic datasets. 18 TNBC samples were collected and utilized to verify the association between gene expression and immune cell infiltration by multiplex immunohistochemistry (mIHC). A specific type of cellular senescence was found to be significantly associated with response to ICB in TNBC. We employed the expression of four senescence-related genes, namely *CDKN2A*, *CXCL10*, *CCND1*, and *IGF1R*, to define a distinct senescence-related classifier using the non-negative matrix factorization approach. Two clusters were identified, namely the senescence-enriching cluster (C1; *CDKN2A*^{high}*CXCL10*^{high}*CCND1*^{low}*IGF1R*^{low}) and proliferating-enriching cluster (C2; *CDKN2A*^{low}*CXCL10*^{low}*CCND1*^{high}*IGF1R*^{high}). Our results indicated that the C1 cluster responds better to ICB and behaves with higher $CD8^+$ T cell infiltration than the C2 cluster. Altogether, in this study, we developed a robust cellular senescence-related classifier of TNBC based on the expression of *CDKN2A*, *CXCL10*, *CCND1*, and *IGF1R*. This classifier act as a potential predictor of clinical outcomes and response to ICB.

Keywords: Immune checkpoint blockade, cellular senescence, triple-negative breast cancer, scRNA-seq, bioinformatics

Introduction

Immune checkpoint blockade (ICB) has led to great success in treating patients with several types of solid tumors, such as melanoma [1] and lung cancer [2]. However, only about 10-30% of patients benefit from it [3-5]. This observation highlights the importance of understanding molecular heterogeneity and biomarker research for identifying phenotypes that exhibit an improved response to ICB.

Combining ICB with chemotherapy has increased the response rates to therapy in patients with triple-negative breast cancer (TNBC) [6, 7]. TNBC, with a high tumor mutational burden and high immune infiltration, responds better to ICB than luminal breast cancer [8, 9]. Nevertheless,

Table 1. Information of datasets used in this study

Datasets	Available omics	ICB	Source
METABRIC cohort	Transcriptomics	No	Curtis et al., 2012
TCGA-BRCA cohort	Transcriptomics	No	Cancer Genome Atlas Network, 2012
GSE173839 cohort	Transcriptomics	Yes	Pusztai et al., 2021
GSE58812 cohort	Transcriptomics	No	Jezequel et al., 2015
GSE124821 cohort	Transcriptomics	Yes	Hollern et al., 2019
Bassez cohort 1	ScRNA-seq	Yes	Bassez et al., 2021
GSE75688 cohort	ScRNA-seq	No	Chung et al., 2017
GSE176078 cohort	ScRNA-seq	No	Wu et al., 2021
PDC000120 cohort	Proteomics	No	Krug et al., 2020
PDC000173 cohort	Proteomics	No	Mertins et al., 2016

ICB, immune checkpoint blockade.

the benefits of ICB in TNBC are limited, and which TNBC subgroup may benefit the most from ICB has not yet been determined. Thus, precisely identifying biomarkers for patients with TNBC who respond well to ICB is crucial.

Cellular senescence is a permanent state of cell cycle arrest that plays a dual role in tumor immunity [10, 11]. On the one hand, senescent cells exhibit a protective effect against tumorigenesis by enhancing immune clearance and tissue remodeling [12]. On the other hand, the senescence-associated secretory phenotype (SASP) factors released by the senescent cells suppress tumor immunity [13, 14]. Therefore, further comprehensively analyzing the associations between cellular senescence and tumor immunity in TNBC is essential.

Infiltration of $CD3^+$ T cells and $CD8^+$ T cells, PD-1/PD-L1 expression, and tumor mutation burden are important determinants of response to ICB. SASP could be utilized by senescent tumor cells to influence the effect of ICB. The combination of ICB and senolytic has been used to increase immune surveillance in some special cancer types such as KRAS-mutant pancreatic ductal adenocarcinoma [15], CDK4/CDK6 inhibitor responsive melanoma [16], and brain metastatic breast cancer [17]. However, the relationship of senescence phenotype and response to ICB in TNBC is still unclear. As a result, exploring specific senescence-related biomarkers in TNBC patients may accurately identify patients who will benefit from ICB.

In this study, we aimed to define a distinct cellular senescence-related classifier and identify potential subtype-specific vulnerabilities of ICB in TNBC by integrated analysis of three scRNA-seq cohorts and multiple bulk RNA sequencing cohorts. The findings of our study may give aid to elucidate the senescence-related heterogeneity in TNBC at both the single-cell and bulk levels.

Materials and methods

ICB cohorts

To investigate and verify the association between cellular senescence and tumor immunity, breast cancer (BC) cohorts with ICB response or T cell expansion information and transcriptomic data were analyzed at bulk and single-cell levels. Data of the single-cell cohort (Bassez cohort 1) [18] were publicly available at http://biokey.lambrechtslab.org (**Table 1**). Data of the bulk cohorts were accessed through GEO accession numbers GSE173839 [19] and GSE124821 [20] (**Table 1**).

Non-ICB cohorts

To compare the immune cell infiltration and senescence heterogeneity between two clusters, multiple cohorts without ICB information were analyzed at transcriptomic and proteomic levels. Transcriptomic data of The Cancer Genome Atlas-BRCA (TCGA-BRCA) cohort were downloaded from the UCSC Xena data portal (https://xenabrowser.net) [21], while those of the METABRIC cohort were downloaded from cBioPortal (https://www.cbioportal.org) [22-24] (**Table 1**). Data of the other transcriptomic cohorts at the bulk and single-cell levels were accessed through GEO accession numbers GSE58812 (bulk) [25], GSE75688 (single-cell)

[26], and GSE176078 (single-cell) [27] (**Table 1**). Data from two proteomic cohorts were downloaded from the National Cancer Institute's Clinical Proteomic Tumor Analysis Consortium (CPTAC) portal (https://proteomic.datacommons.cancer.gov/pdc/) through accession numbers PDC000120 [28] and PDC000173 [29] (**Table 1**). Two proteomic cohorts were merged as an independent proteomic cohort, and "combat" was used to remove the batch effect.

scRNA-seq data analysis

Bassez cohort 1 and GSE75688 datasets contain annotated cell types of each sample. Data of cancer cells from patients with TNBC were analyzed in the Bassez cohort 1 dataset, whereas those of cancer cells from all patients with BC were analyzed in the GSE75688 dataset. In the GSE176078 dataset, data from patients with TNBC were analyzed using the Seurat package [30]. Epithelial cells could be recognized based on the following characteristics: KRT19+ and PTPRC-. In contrast, $CD4^+$ T cells, $CD8^+$ T cells, naïve T cells, and Treg cells were classified and recognized by Uniform Manifold Approximation and Projection (UMAP) [31] based on CD4, CD8A, CCR7, and FOXP3 expression, respectively. The "harmony" package was used to remove the batch effect [32]. UCell method was used to calculate the subtype score based on specific genes [33].

Transcriptomic and proteomic data analysis at the bulk level

The "limma" package [34] was used to identify differentially expressed genes (DEGs) between ICB-treated patients with pathological complete remission (pCR) and those without pCR in the GSE173839 dataset. Genes with |log fold change| ≥ 0.85 and false discovery rate < 0.05 were regarded as DEGs. We used DEGs as input to perform the Kyoto Encyclopedia of Genes and Genomes (KEGG) analysis via Metascape online tools [35] (https://metascape.org/gp/index.html#/main/step1) with minimum overlap = 5, minimum enrichment = 3, and *P*-value < 0.05. The senescence-related gene list comprised genes from hsa04218, GO: 0090398, and a core panel of frailty biomarkers [36] (Table S1). Transcriptomic data of the GSE173839 dataset was used to define distinct senescence-related classifiers by the non-negative matrix factorization (NMF) approach [37]. Furthermore, transcriptomic data of the TCGA-TNBC, METABRIC-TNBC, GSE58812, GSE75688, GSE124821 datasets, and proteomic data were used to verify the classifiers. The "IOBR" package [38] was used to evaluate immune cell infiltration in the GSE173839, TCGA-TNBC, METABRIC-TNBC, GSE58812, and GSE75688 datasets by performing CIBERSORT [39], ESTIMATE [40], Xcell [41], MCPCounter [42], quanTIseq [43], EPIC [41], and TIMER [44] analysis. Gene Set Enrichment Analysis (GSEA) analysis [45] was employed to identify the cluster exhibiting senescence-enriched phenotypes in the TCGA-TNBC, METABRIC-TNBC, GSE58812, and proteomic datasets with the list of senescence-related gene set downloaded from KEGG website (Table S1: hsa04218). The immunophenoscores (IPS) of the TCGA-TNBC cohort used to predict the efficacy of ICB were downloaded from The Cancer Immunome Atlas database (https://tcia.at/home) [46, 47].

Patients and tissue microarray specimens

Formalin-fixed paraffin-embedded tissue blocks were collected from the Affiliated Hospital of Jining Medical University, China. Tissues were collected from patients with TNBC who received no chemotherapy or radiotherapy. For tissue microarray construction, all specimens were re-evaluated using hematoxylin and eosin staining, and the representative areas were selected and constructed into 2.0 mm tissue cores. In this study, a total of 18 cases were analyzed (Table S2). All of the research was reviewed and approved by the Ethics Committee of the Affiliated Hospital of Jining Medical University (approval number: 2021-08-C015). Informed consent was obtained from all subjects involved in the study.

mIHC assay development and staining

Tissue microarray slides were dewaxed in xylene and rehydrated by graded ethanol solutions, followed by 1-hour baking at 65°C. Antigen retrieval was performed using a high-pressure heat method with sodium citrate solution (pH = 6). After cooling down to room temperature, the slides were blocked and incubated with the IGF1R antibody (Abcam, ab263903, 1:600) at room temperature for 1 h. Subsequently, secondary antibodies and Opal 520 fluorophores (NEL811001KT, Akoya)

were incubated at room temperature for 10 min after washing with TBST thrice. Slides stained using IGF1R-Opal 520 were retrieved by microwave oven with sodium citrate solution (pH = 6). After cooling down to room temperature, the slides were blocked and incubated with the other three antibodies and Opal fluorophores (CXCL10-Opal 690, PTG, 10937-1-AP, 1:300; CD3-570, PTG, 17617-1-AP, 1:1000; CD8-620, PTG, 66868-1-Ig, 1:6000). Staining was performed using DAPI as per the standard procedure. mIHC Slides were scanned by Vectra Polaris and pictures were captured by Vectra Polaris 1.0.10. The ratio of marker-positive cells was calculated by QuPath software [48].

Statistical analysis

Statistical analyses were generated using R v4.1.3 (https://www.r-project.org) or GraphPad Prism 9 (https://www.graphpad.com/). A comparison of immune cell infiltration scores and expression of SASP factors between two groups was analyzed using two-sided Wilcoxon tests. Categorical variables were compared between two groups or more than two groups using the Chi-square test or Fisher's exact test. The receiver operating characteristic (ROC) curve was used to evaluate predictive performance. Kaplan-Meier plots of OS, progression-free interval (PFI), and metastasis-free survival (MFS) were performed using GraphPad Prism 9. Values of $P < 0.05$ using the Gehan-Breslow-Wilcoxon test were used to define differences in survival time.

Results

Identifying core senescence-related genes that correlated with response to ICB

To investigate the biomarkers for ICB, we identified DEGs between data of patients who responded to ICB and those who did not respond to ICB in the GSE173839 dataset (**Figure 1A**). For analysis of pathway enrichment using DEGs as input, pathways such as IL17 signaling pathway, p53 signaling pathway, chemokine signaling pathway, and cellular senescence that had been reported to regulate the immune system and inflammatory response in the progressive of various diseases were enriched (**Figure 1B**). As reported before, cellular senescence was mediated by the p53 signal pathway [49, 50] and SASP was mediated by the IL17 signaling pathway [51, 52] and the chemokine signaling pathway [53, 54]. Although the senescence-related pathway is not the most significantly enriched in the list, the other pathways are connected with the cellular senescence signal pathway closely. As a result, the association between cellular senescence and ICB response was further explored. The six most significant senescence-related DEGs (**Figure 1C**) were selected for further validation in the scRNA-seq cohort (**Figure 1D**). Among them, the expression of *CDKN2A*, *CXCL10*, *CCND1*, and *IGF1R* in the TNBC cancer cells was associated with T cell expansion (**Figure 1E**). UCell score based on the four genes of each cancer cell was remarkablely different between the TNBC samples with (E group) and without (NE group) T cell expansion (**Figure 1F**). This result demonstrated that the E group had a higher four-gene score than the NE group (**Figure 1G**).

Defining and verifying a classifier of TNBC based on CDKN2A, CXCL10, CCND1, and IGF1R expression

Consensus clustering analysis of the NMF algorithm was used to identify distinct senescence pattern clusters based on the expression of *CDKN2A*, *CXCL10*, *CCND1*, and *IGF1R* in the GSE173839 dataset. Two clusters were identified as k = 2 when the magnitude of the cophenetic correlation coefficient began to decrease, including 41 cases in cluster C1 and 30 cases in cluster C2 (**Figure 2A**). The heatmap plot exhibited the consensus matrix of NMF clustering results using transcriptomic data in the GSE173839 dataset (**Figure 2B**). The C1 cluster exhibited higher expression of *CDKN2A* and *CXCL10* and lower expression of *CCND1* and *IGF1R* than the C2 cluster (**Figure 2C**). Meanwhile, the proportion of patients with pCR was higher in the C1 cluster than in the C2 cluster (**Figure 2D**). The immune infiltration score calculated using ESTIMATE (**Figure 2E**) and xCELL (**Figure 2F**) indicated that the C1 cluster had more immune activity than the C2 cluster. For further validation, three transcriptomic data samples of the TNBC cohorts were used to verify the senescence pattern clusters constructed based on the GSE173839 cohort. The results indicated that the C1 cluster had higher expression of *CDKN2A* and *CXCL10* and lower expression of *CCND1* and *IGF1R* than the C2

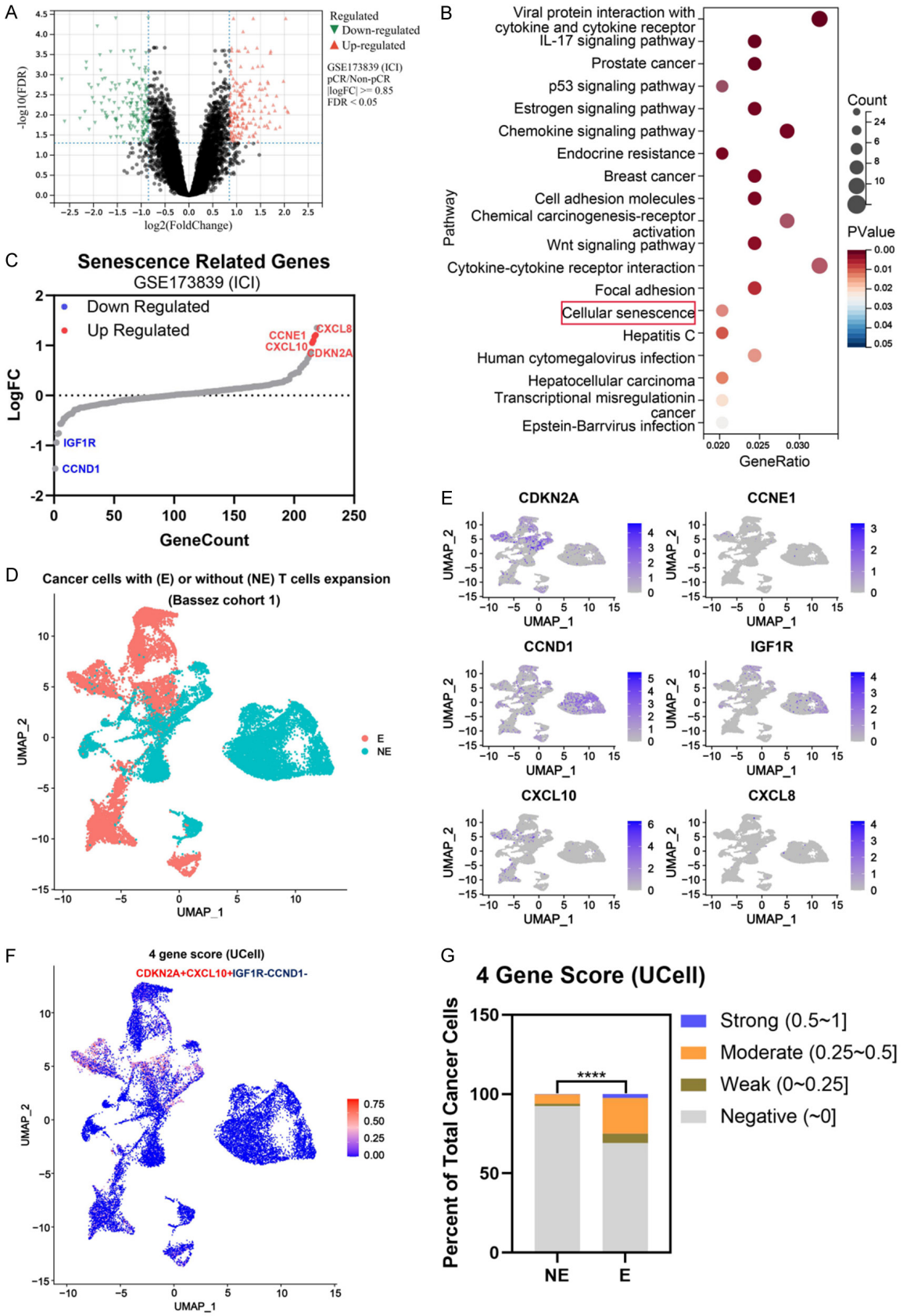

Figure 1. Identification of genes correlated with immune checkpoint blockade response. A. Volcano plot depicted the differentially expressed genes (DEGs) between patients in the pathological complete regression (pCR) group and that in the non-pCR group using transcriptomics data from the GSE173839 dataset. B. Bubble plot of Kyoto

Encyclopedia of Genes and Genomes analysis using DEGs as input showed that cellular senescence pathway was enriched. C. Six senescence-related genes, including CDKN2A, CXCL10, CCND1, IGF1R, CXCL8, and CCNE, were identified as DEGs in the GSE173839 dataset. D. Uniform Manifold Approximation and Projection (UMAP) plot of cancer cells between triple-negative breast cancer (TNBC) patients with T cell expansion (E) and TNBC patients without T cell expansion (NE) using scRNA-seq data from Bassez cohort 1. E. UMAP plot showed that the expressions of CDKN2A, CXCL10, CCND1, and IGF1R were significant difference between cancer cells in the E group and cancer cells in the NE group. F. UMAP plot of UCell score based on the expressions of CDKN2A, CXCL10, CCND1, and IGF1R in cancer cells derived from TNBC patients. G. Cancer cells in the E group had stronger UCell scores based on the expressions of CDKN2A, CXCL10, CCND1, and IGF1R than cancer cells in the NE group. DEGs, differentially expressed genes; pCR, pathological complete regression; Uniform Manifold Approximation and Projection, UMAP; triple-negative breast cancer, TNBC; ****P < 0.0001.

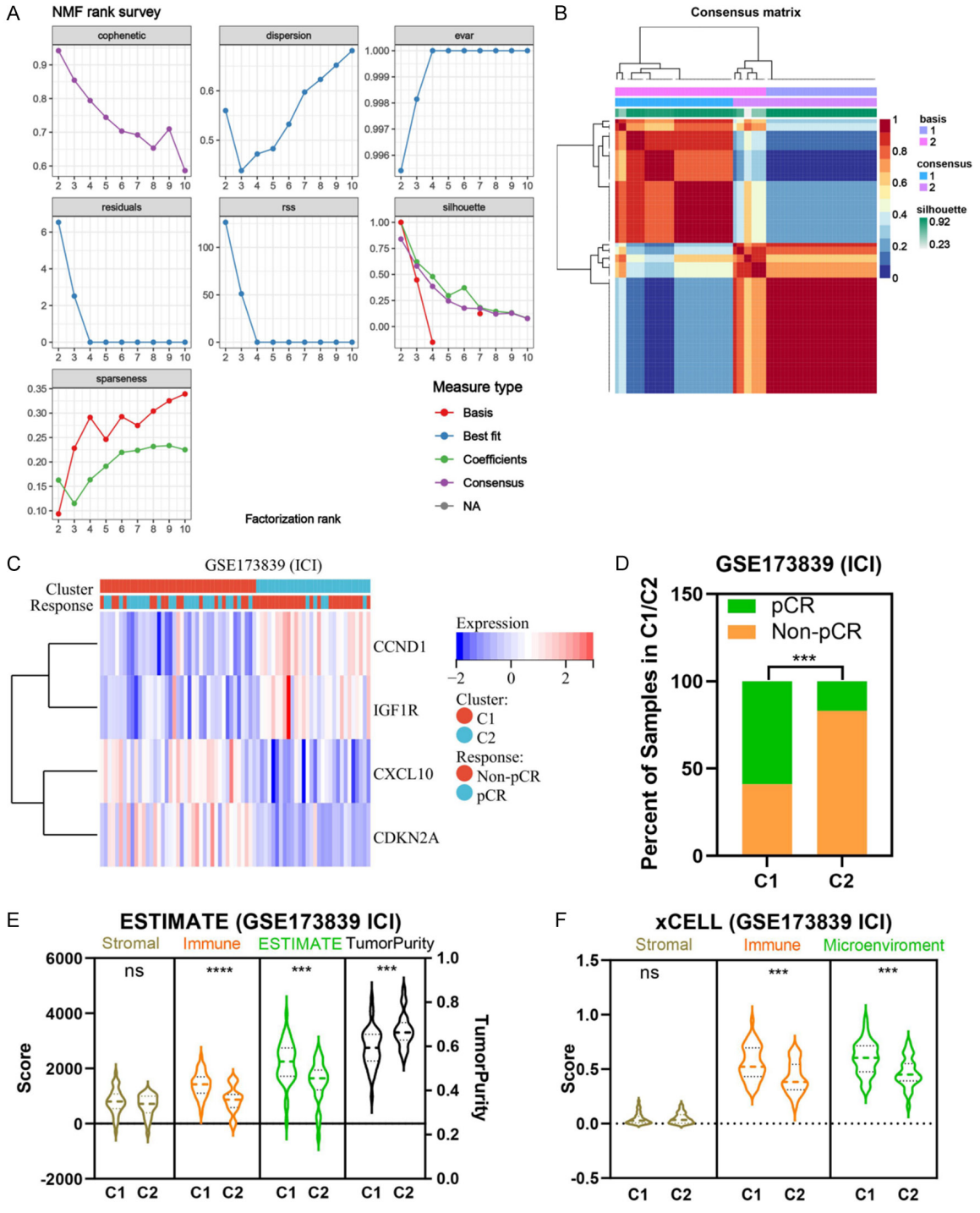

Figure 2. Development of senescence-related classifier by Non-negative Matrix Factorization Approach (NMF) using data from the GSE173839 dataset. A. NMF rank survey indicated the number of clusters should be equal to 2. B. The heatmap plot exhibited the consensus matrix of NMF clustering results. C. The heatmap plot exhibited the expressions of CDKN2A, CXCL10, CCND1, and IGF1R between C1 and C2. D. The bar plot showed the percent of patients with pathological complete regression (pCR) in C1 was higher than that in C2. E. The bar plot showed patients in C1 had higher ESTIMATE immune scores than that in C2. F. The bar plot showed patients in C1 had higher xCell immune scores than that in C2. NMF, Non-negative Matrix Factorization Approach; pCR, pathological complete regression; ***P < 0.001.

cluster in protein level in the TCGA-TNBC, GSE58821, and METABRIC-TNBC cohorts (**Figure 3A-C**). Similarly, the C1 cluster displayed higher immune infiltration levels than the C2 cluster in three cohorts (**Figure 3D-I**). Moreover, patients in the C1 cluster had better OS (**Figure 3J**) and PFI (**Figure 3K**) than those in the C2 cluster in the TCGA-TNBC cohort. Furthermore, patients in the C1 cluster had better OS (**Figure 3L**) and MFS (**Figure 3M**) than those in the C2 cluster in the GSE58821 cohort.

Verifying the classifier of TNBC at the single-cell level

Eleven primary BC tumor samples in the GSE75688 cohort were subjected to bulk RNA-seq and scRNA-seq. Firstly, we continuously divided these 11 patients into C1 and C2 clusters by NMF using data at the bulk level (**Figure 4A**). The C1 cluster was also found to contain a higher expression of *CDKN2A* and *CXCL10*, a higher immune score, and a lower expression of *CCND1* and *IGF1R* than those in the C2 cluster (**Figure 4A** and **4B**). Secondly, we evaluated the expression of four genes and the four-gene score of the same patients using data at the single-cell level (**Figure 4C-E**). The four-gene score was calculated by UCell algorithm which is the more appropriate method for evaluating the pathway or multiple-gene score when using data at the single-cell level. The patients with a higher four senescence-related gene score may be closer to patients with a senescence phenotype as well as patients in the C1 cluster. Our results demonstrated that cancer cells in the C1 cluster have a higher four-gene score than those in the C2 cluster at the single-cell level (**Figure 4F**), which further validated the robustness of our classifier.

$CD8^+$ T cell infiltration difference between patients with TNBC in C1 and C2 clusters

CIBERSORT, MCPCounter, quanTIseq, EPIC, and TIMER analysis were used to evaluate the infiltration abundance of $CD8^+$ T cells in the TCGA-TNBC, GSE58812, and METABRIC-TNBC cohorts at the bulk level. Our results indicated that the C1 cluster had a higher proportion of $CD8^+$ T cells than the C2 cluster in the TCGA-TNBC (**Figure 5A**), GSE58812 (**Figure 5B**), and METABRIC-TNBC (**Figure 5C**) cohorts. TNBC data in the GSE176078 cohort was analyzed at the single-cell level (**Figure 6A**). We first calculated the four-gene score of each PTPRC-KRT19+ epithelial cell based on the expression of *CDKN2A*, *CXCL10*, *CCND1*, and *IGF1R* by the UCell algorithm (**Figure 6A-C**). The cells with a four-gene score > 0 were regarded as senescence-positive cells and patients with a proportion of senescence-positive cells in total epithelial cells > 50% were categorized to the C1 cluster, whereas others were categorized to the C2 cluster (**Figure 6C**). We then classified and recognized $CD4^+$ T cells, $CD8^+$ T cells, naïve T cells, and Treg cells from total $CD3^+$ T cells of patients in the C1 and C2 clusters (**Figure 6D** and **6E**). The results indicated that patients with TNBC in the C1 cluster had a higher infiltration abundance of $CD8^+$ T cells than those in the C2 cluster at the single-cell level (**Figure 6F**).

Essentially, mIHC staining was conducted to verify the co-expression of CXCL10 and IGF1R with CD3 and CD8 in 18 TNBC PPFE samples. Here, CXCL10 was marked red, IGF1R was marked green, CD3 was marked orange, CD8 was marked yellow, and DAPI was marked blue (**Figure 7A**). Results indicated that the patient with $CXCL10^{high}IGF1R^{low}$ had stronger staining intensity of CD3 and CD8 than the patient with $CXCL10^{low}IGF1R^{high}$ (**Figure 7A**). In addition, we found the ratio of CXCL10-positives cells is positively correlated with the ratio of CD3-positive cells (**Figure 7B**) and CD8-positive cells (**Figure 7C**). However, the ratio of IGF1R-positive cells is negatively correlated with the ratio of CD3-positive cells (**Figure 7D**) and CD8-positive cells (**Figure 7E**).

Senescence-enriching phenotype of the C1 cluster

We identified biomarkers between epithelial cells from patients in the C1 cluster and epithelial cells from patients in the C2 clusters in the

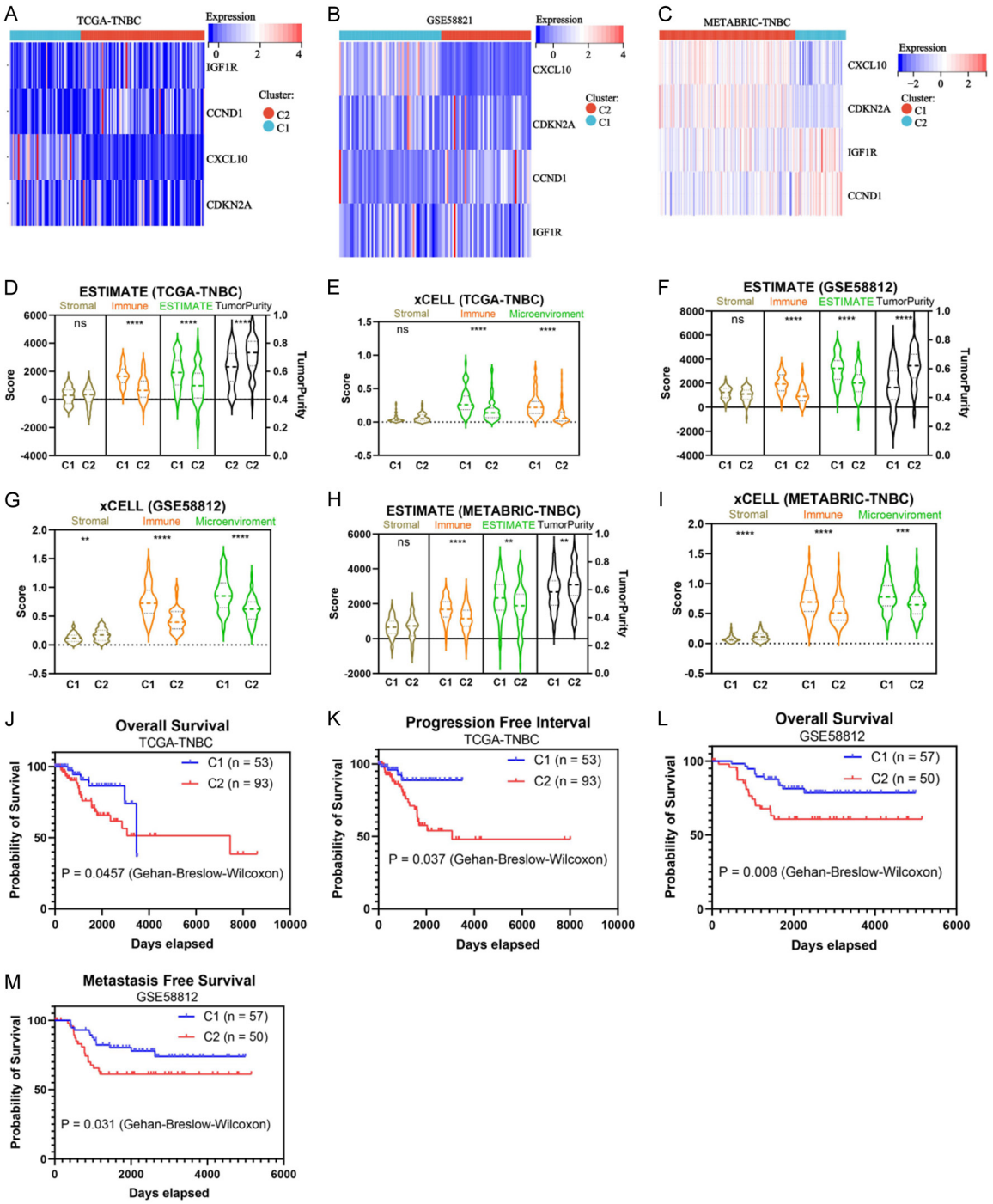

Figure 3. Validation of the senescence-related classifier using data from three transcriptomics datasets at the bulk level. (A-C) The heatmap plot exhibited the expressions of CDKN2A, CXCL10, CCND1, and IGF1R between C1 and C2 using data from the TCGA-TNBC (A), GSE58812 (B), and METABRIC-TNBC (C) dataset, respectively. (D, E) The bar plot showed patients in C1 had higher ESTIMATE immune scores (D) and xCell immune scores (E) than that in C2 using data from the TCGA-TNBC dataset. (F, G) The bar plot showed patients in C1 had higher ESTIMATE immune scores (F) and xCell immune scores (G) than that in C2 using data from the GSE58812 dataset. (H, I) The bar plot showed patients in C1 had higher ESTIMATE immune scores (H) and xCell immune score (I) than that in C2 using data from the METABRIC-TNBC dataset. (J, K) The Kaplan-Meier curve plot showed patients in C1 had longer overall survival (OS) (J) and progress free survival (K) than that in C2 using data from the TCGA-TNBC dataset. (L, M) The Kaplan-Meier curve plot showed patients in C1 had longer OS (L) and metastasis free survival (M) than that in C2 using data from the GSE58812 dataset. TNBC, triple-negative breast cancer; OS, overall survival.

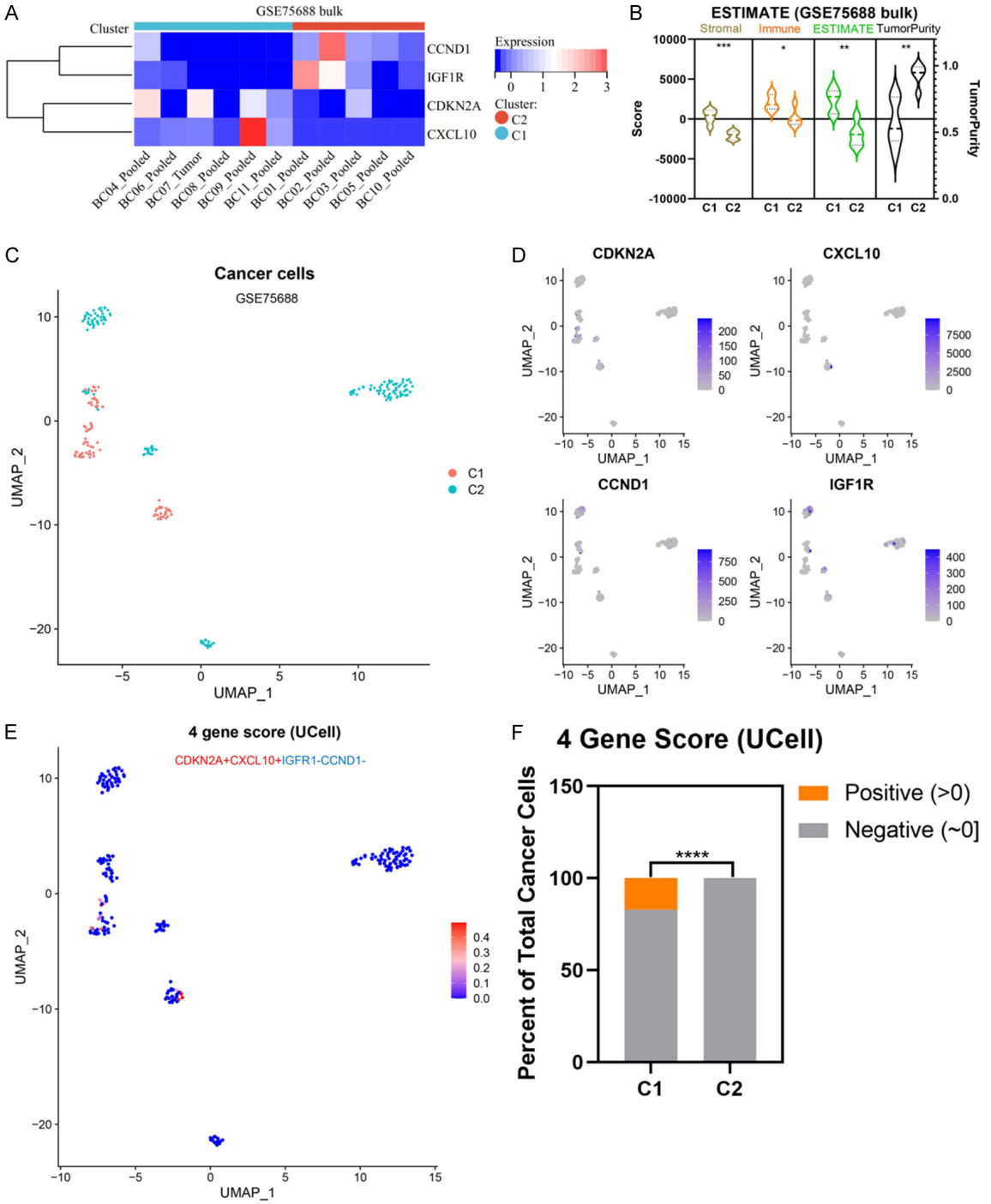

Figure 4. Validation of the senescence-related classifier using transcriptomics data at the single-cell level. A. The heatmap plot exhibited the expressions of CDKN2A, CXCL10, CCND1, and IGF1R between C1 and C2 using bulk-RNA-seq data from the GSE75688. B. The bar plot showed patients in C1 had higher ESTIMATE immune scores than that in C2 using bulk-RNA-seq data from the GSE75688. C. Uniform Manifold Approximation and Projection (UMAP) plot of cancer cells between C1 cluster and C2 cluster using scRNA-seq data from the GSE75688. D. UMAP plot showed the expressions of CDKN2A, CXCL10, CCND1, and IGF1R in cancer cells. E. UMAP plot of UCell score based on the expressions of CDKN2A, CXCL10, CCND1, and IGF1R in cancer cells. F. Cancer cells in C1 cluster had stronger UCell scores based on the expressions of CDKN2A, CXCL10, CCND1, and IGF1R than cancer cells in C2 cluster. UMAP, Uniform Manifold Approximation and Projection; ****P < 0.0001.

GSE176078-TNBC cohort (**Figure 8A**). KEGG analysis using these markers as input showed that the cellular senescence pathway was enriched at the single-cell level (**Figure 8B**). The

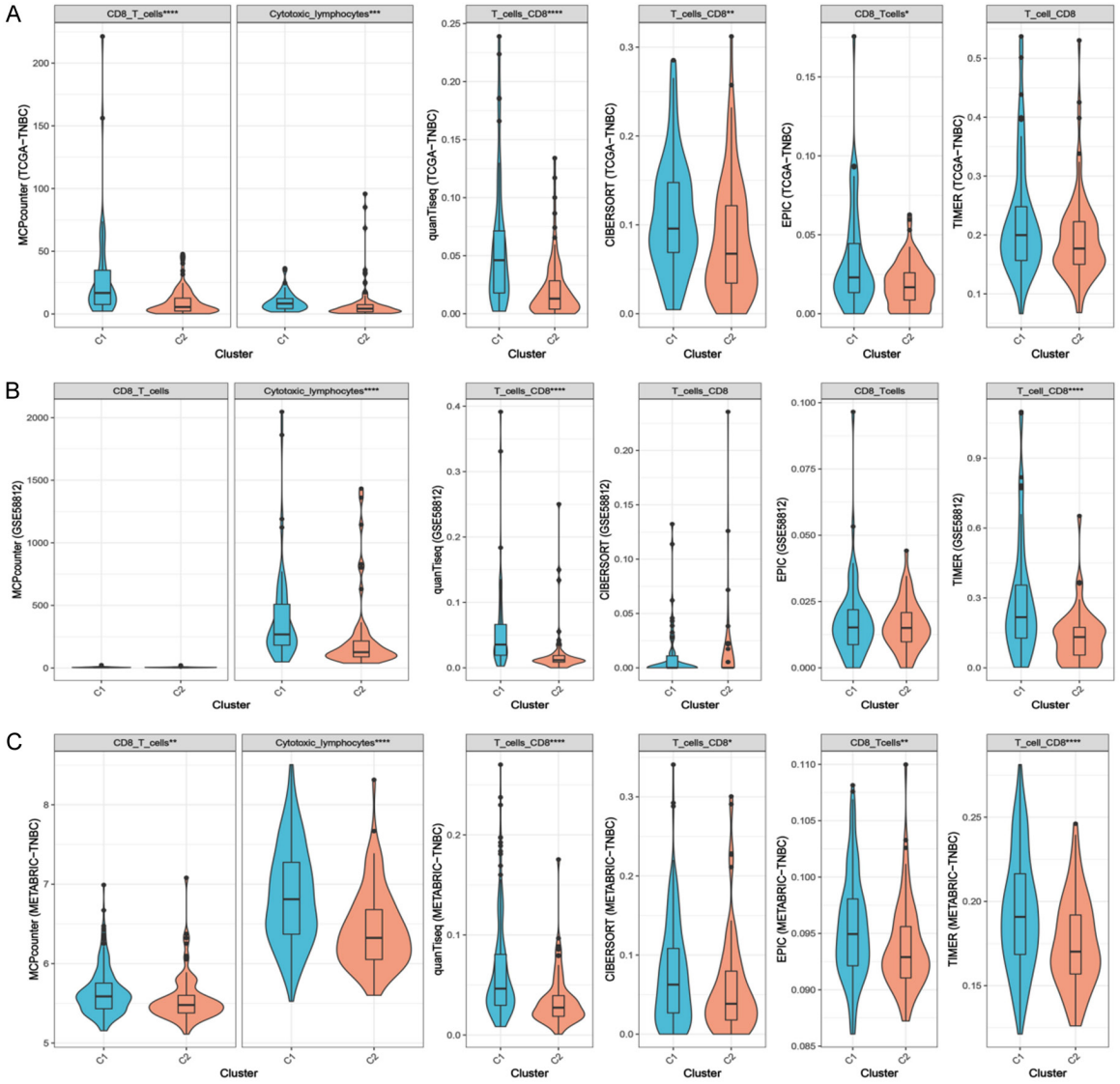

Figure 5. Exploration of the infiltration of $CD8^+$ T cells between C1 and C2 using bulk-RNA-seq data by MCPcounter, quanTiseq, CIBERSORT, EPIC and TIMER methods. A. The violin plot showed samples in C1 had higher infiltration level of $CD8^+$ T cells than that in C2 using data from the TCGA-TNBC dataset. B. The violin plot showed samples in C1 had higher infiltration level of $CD8^+$ T cells than that in C2 using data from the GSE58812 dataset. C. The violin plot showed samples in C1 had higher infiltration level of $CD8^+$ T cells than that in C2 using data from the METABRIC-TNBC dataset. TNBC, triple-negative breast cancer.

GSEA analysis using data from the TCGA-TNBC, GSE58812, and METABRIC-TNBC cohorts revealed that the C1 cluster exhibited a senescence-enriching phenotype at the bulk level (**Figure 8C**). Similarly, data from one merged proteomic cohort were analyzed. We found that the C1 cluster exhibited a senescence-enriching phenotype and higher expression of *CDKN2A* and *CXCL10* and lower expression of *CCND1* and *IGF1R* than the C2 cluster at the protein level (**Figure 8D**).

MMP12 were higher in the C1 cluster than in the C2 cluster (**Figure 8F**). Meanwhile, the expression of the growth factor IGFBP4 was lower in the C1 cluster than in the C2 cluster at the transcriptomic and proteomic levels (**Figure 8E** and **8F**).

Sensitivity of $CDKN2A^{high}CXCL10^{high}CCND1^{low}IGF1R^{low}$ patients with TNBC to ICB

To validate the reliability of our classifier in predicting ICB efficacy, the IPS score of TCGA-TNBC

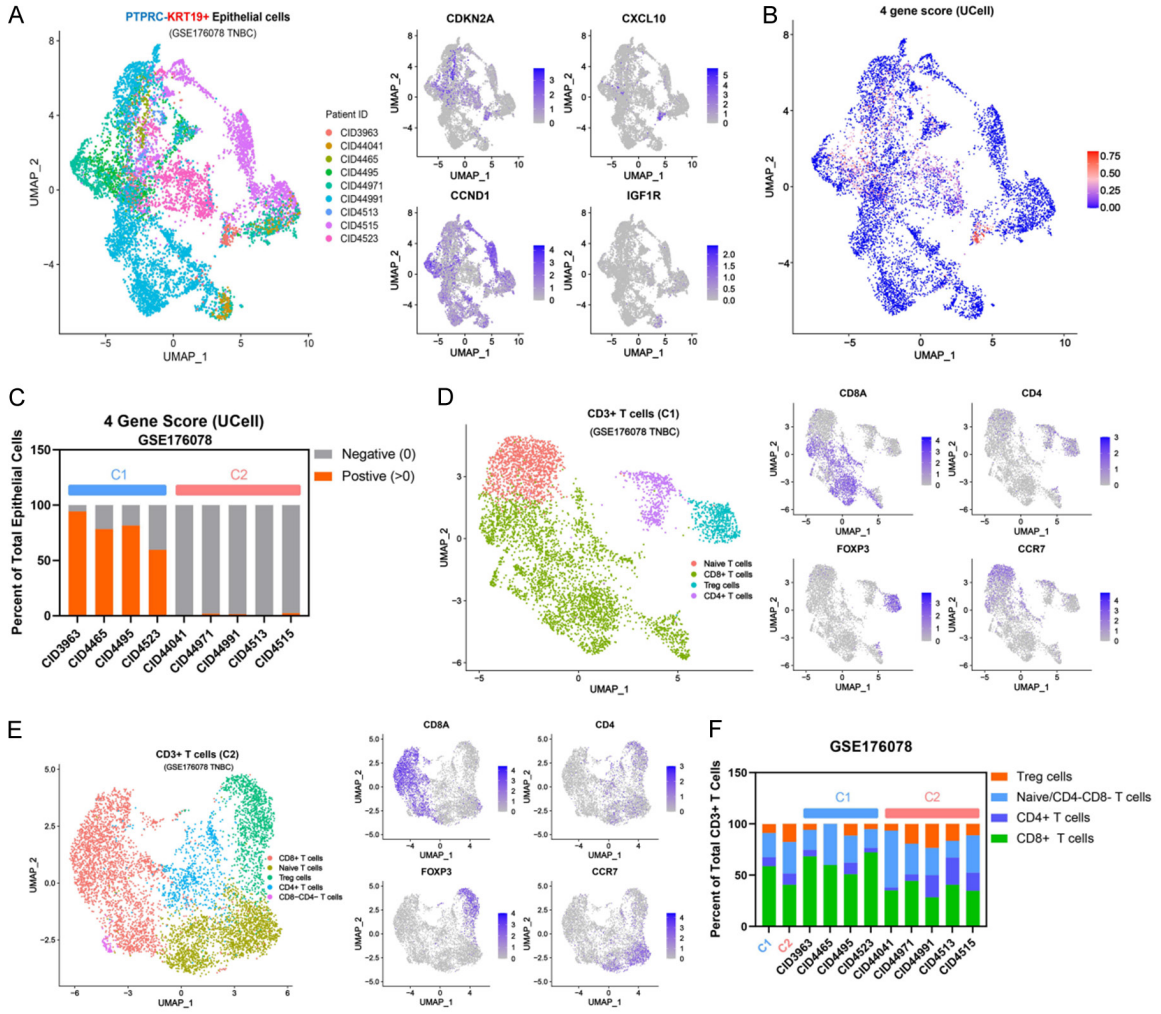

Figure 6. Exploration of the infiltration of CD8$^+$ T cells between C1 and C2 using scRNA-seq data from the GSE176078 dataset. A. Uniform Manifold Approximation and Projection (UMAP) plot of epithelial cells derived from TNBC patients. B. UMAP plot of UCell scores based on the expressions of CDKN2A, CXCL10, CCND1, and IGF1R in epithelial cells. C. The TNBC patients were divided as C1 and C2 clusters according to the percent of UCell-score-positive cells. D. UMPA plot of CD3$^+$ T cells derived from TNBC patients in C1 cluster. E. UMPA plot of CD3$^+$ T cells derived from TNBC patients in C2 cluster. F. The bar plot showed TNBC patients in C1 cluster had higher infiltration level of CD8$^+$ T cells than that in C2 using data at the single-cell level. UMAP, Uniform Manifold Approximation and Projection; TNBC, triple-negative breast cancer.

samples and a mouse transcriptomic dataset (GSE124821) containing information on ICB treatment were analyzed. Our results showed that samples in the C1 cluster had higher IPS scores than those in the C2 cluster using data from the TCGA-TNBC cohort, indicating that the C1 cluster patients received more benefits from ICB than the C2 cluster patients (**Figure 9A**). Moreover, we found that the ICB-sensitive samples exhibited higher expression of *Cdkn2a* and *Cxcl10* and lower expression of *Ccnd1* and *Igf1r* than the ICB-resistant samples (**Figure 9B**) in the GSE124821 cohort. Besides, we divided samples into the C1 cluster (*Cdkn2a*^{high}*Cxcl10*^{high}) and the C2 cluster (*Ccnd1*^{high}*Igf1r*^{high}) by NMF based on the mRNA expression of the four senescence-related genes in the GSE124821 cohort (**Figure 9C**). Our result demonstrated that a higher proportion of samples sensitive to ICB was seen in the C1 cluster than in the C2 cluster (**Figure 9D**). Then we performed ROC analysis using "pROC" package. In detail, the senescence-related cluster status (C1 or C2) and status of response to ICB (sensitive or resistant) of these samples were used for performing ROC analysis and calculating the area under the curve (AUC) value. The ROC analysis indicated

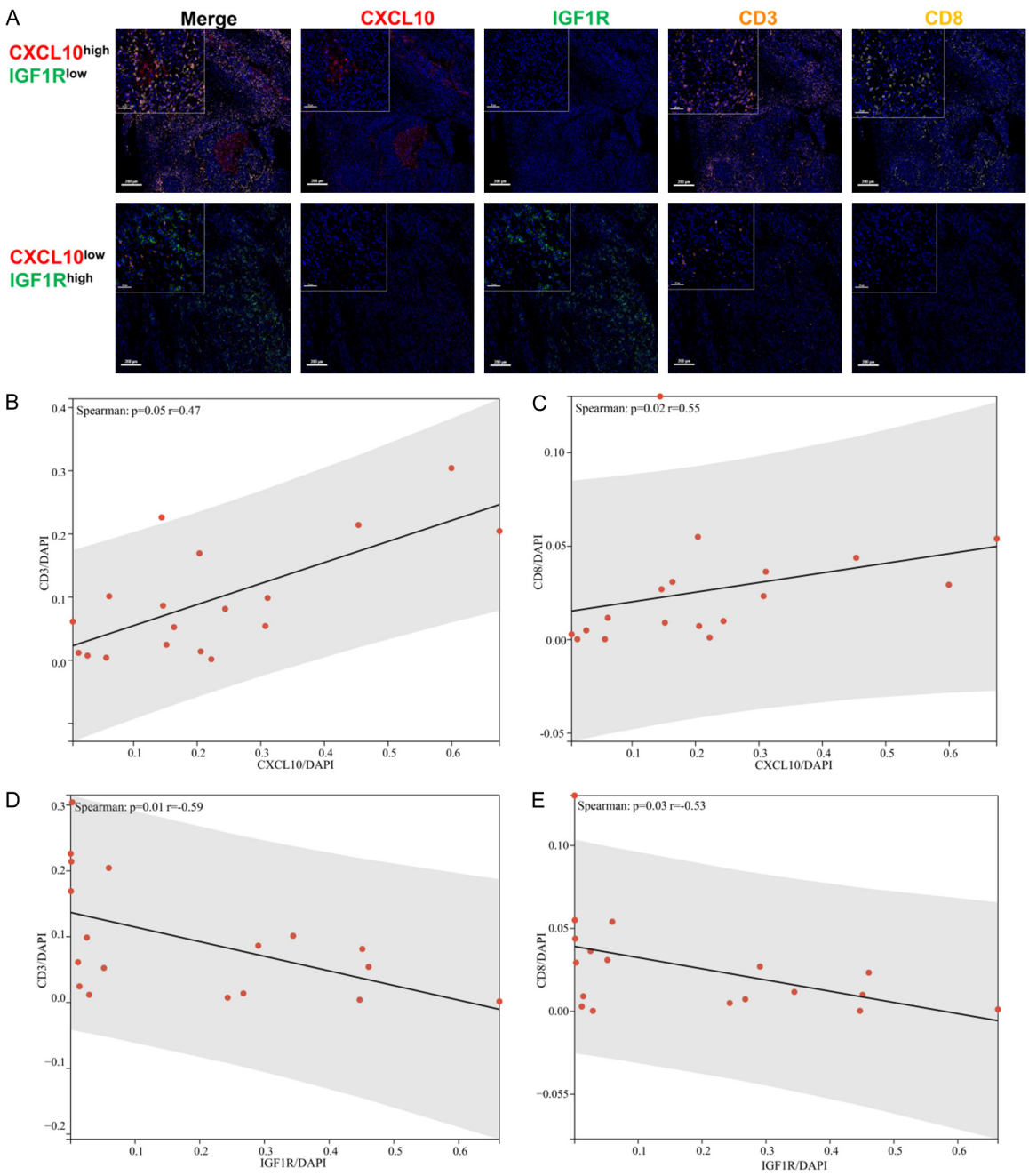

Figure 7. Multiplex immunofluorescence staining analysis of CXCL10 and IGF1R co-expression with CD3 and CD8 in 18 triple-negative breast cancer samples. A. Two cases of multiplex immunofluorescence staining of CXCL10, IGF1R, CD3 and CD8. B. Correlation of CD3 with CXCL10. C. Correlation of CD8 with CXCL10. D. Correlation of CD3 with IGF1R. E. Correlation of CD8 with IGF1R.

that the classifier based on four senescence-related genes predicts the efficacy of ICB remarkably well (area under curve value = 0.79, 95% confidence interval: 0.84-0.74; **Figure 9E**). Similarly, the C1 cluster exhibited a senescence-enriching phenotype and higher expression of SASP factors, such as IL1a, IL1b, IL6, CCL5, and CCL8 than the C2 cluster in the GSE124821 cohort (**Figure 9F** and **9G**).

Discussion

Novel biomarkers identified or validated using gene expression data at single-cell resolution may perform better than those using the traditional RNA-seq data at the bulk level. Our study focused on identifying cellular senescence-related biomarkers for TNBC with different ICB responses at both single-cell and bulk levels.

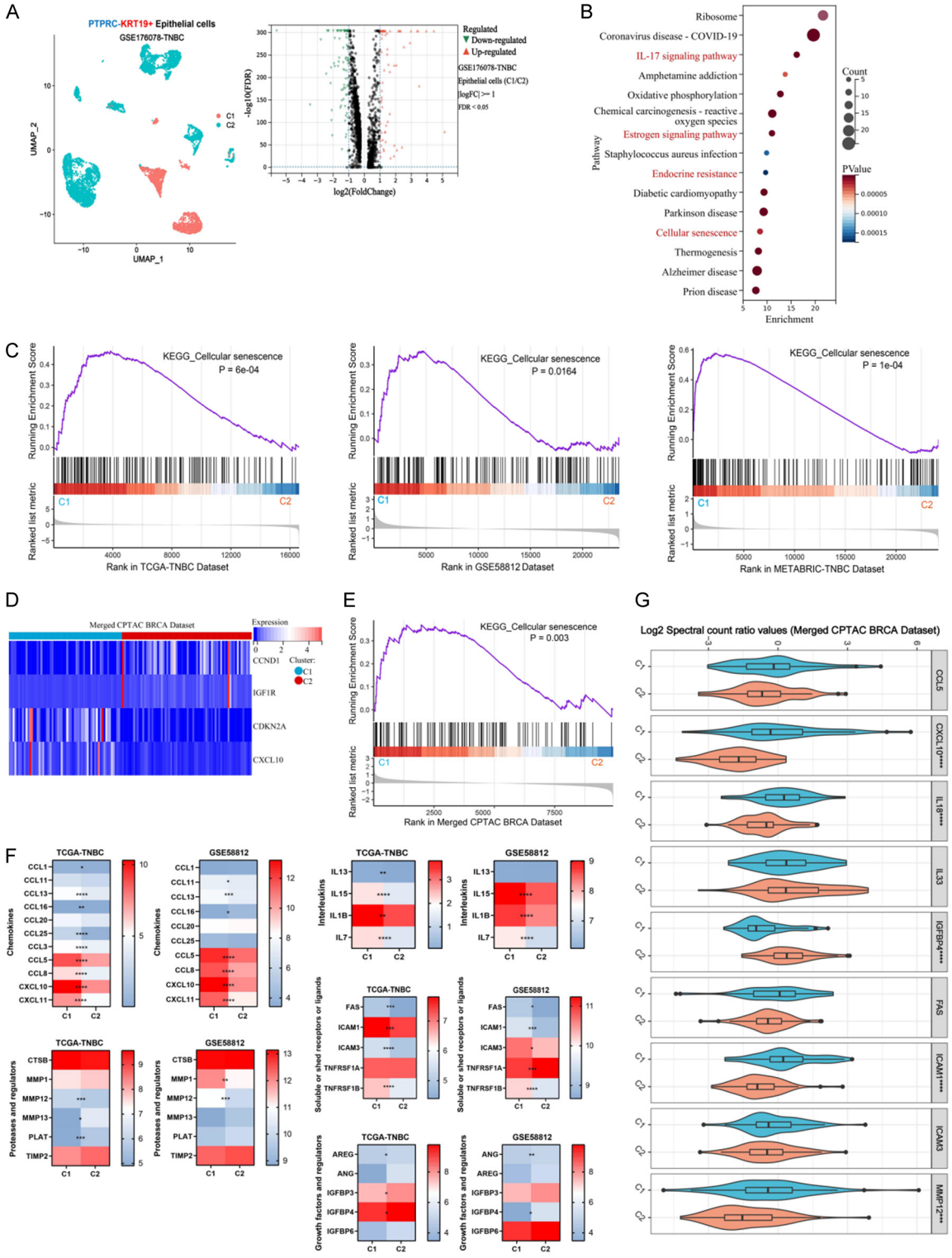

Figure 8. Identification of C1 cluster as a senescence-enriching phenotype. A. Uniform Manifold Approximation and Projection (UMAP) plot and volcano plot depicted the differentially expressed genes (DEGs) between epithelial cells in C1 cluster and epithelial cells in C2 cluster using scRNA-seq data from the GSE176078 dataset. B. Bubble plot of Kyoto Encyclopedia of Genes and Genomes analysis using DEGs as input also showed that cellular senescence pathway was enriched. C. Gene Set Enrichment Analysis (GSEA) plot showed cellular senescence pathway was enriched in C1 cluster using bulk-RNA-seq data from the TCGA-TNBC, GSE58812, and METABRIC-TNBC dataset, respectively. D. The heatmap plot exhibited the proteomics expression levels of CDKN2A, CXCL10, CCND1, and IGF1R between C1 and C2, and GSEA plot showed cellular senescence pathway was enriched in C1 cluster at the protein level. E.

GSEA plot showed cellular senescence pathway was enriched in C1 cluster using data from the merged CPTAC BRCA dataset. F. The heatmap plot exhibited that the transcriptomics expression levels of some senescence-associated secretory phenotype (SASP) factors, such as CCL5, CCL8, IL1B, IL7, MMP7, ICAM1, ICAM3, TNFRSF1B etc., was higher in C1 cluster than that in C2 cluster using data from the TCGA-TNBC and GSE58812 dataset, respectively. G. The violin plot showed the proteomics expression levels of some SASP factors, such as CXCL10, IL18, ICAM1, and MMP12, was higher in C1 cluster than that in C2 cluster using data from the merged CPTAC BRCA dataset. UMAP, Manifold Approximation and Projection; DEGs, differentially expressed genes; GSEA, Gene Set Enrichment Analysis; TNBC, triple-negative breast cancer; SASP, senescence-associated secretory phenotype.

On the one hand, cellular senescence promotes immunosuppression and decreases the efficacy of immunotherapy in glioblastoma [55]. On the other hand, interferon-dependent and cytokine-induced senescence lead to self-sustaining senescence surveillance of melanoma, and patients with metastatic melanoma that lost senescence-inducing genes and amplificated senescence inhibitors progressed rapidly after receiving ICB therapy, suggesting that senescence may play a critical role in killing cancer cells that escape from ICB therapy [56, 57]. Although the interaction between cellular senescence and anti-tumor immunity is complex [10, 11, 58], mounting evidence has highlighted the necessity of understanding the senescent heterogeneity in cancer, which may help to identify biomarkers of ICB [58, 59].

In this study, we developed a robust cellular senescence-related classifier that divided TNBC patients into two clusters (C1 cluster vs C2 cluster) based on the expression of CDKN2A, CXCL10, IGF1R, and CCND1 using non-negative matrix factorization (NMF) approach. Patients in the C1 cluster have high expression levels of CDKN2A and CXCL10 and low expression levels of IGF1R and CCND1, which was a senescence phenotype and predicted a sensitive response to ICB. On the contrary, patients in the C2 cluster expressed low levels of CDKN2A and CXCL10 and high levels of IGF1R and CCND1, which was a proliferation phenotype and predicted a resistant response to ICB.

P16, a tumor suppressor and classical mediator of cellular senescence coded by *CDKN2A*, was associated with a better prognosis in human BC [60]. Loss of p16(Ink4a) has been shown to render BC resistant to endocrine-based therapies [61, 62]. Our study showed that DEGs between ICB responder and non-responder groups (**Figure 1B**) or between patients in cluster C1 and cluster C2 (**Figure 8B**) were enriched in KEGG-endocrine-resistant pathways. This finding indicates that there is complex crosstalk between endocrine-based therapy and ICB. However, research on the association of CDKN2A and anti-tumor immunity is limited. Our results demonstrated that both CDKN2A and CXCL10, as SASP factors, were positively correlated with the infiltration abundance of $CD8^+$ T cells, which were the main cells involved in anti-tumor immunity.

CCND1 is a key regulator of cell cycle and proliferation, and overexpression of CCND1 promotes tumorigenesis, cell proliferation, tamoxifen resistance, and recurrence of BC [63-65]. IGF1/IGF1R signaling regulates cell growth and promotes growth effects in TNBC cells [66]. IGF1R inhibition enhances the effects of chemoimmunotherapy combined with ICB by initiating autophagy and enhancing $CD8^+$ T cell infiltration [67]. In this study, cluster C2 exhibited a high expression of *CCND1* and *IGF1R*, low-immune activity, rare $CD8^+$ T cell infiltration and worse prognosis, which indicated that IGF1R inhibition combined with chemoimmunotherapy, and ICB and might help prolong the OS of TNBC patients.

Our study found that cluster C1 which exhibited a senescence-enriching phenotype and was characterized by high expression of *CDKN2A* and *CXCX10* had high $CD8^+$ T cell infiltration and responsiveness to ICB in multiple datasets at both single-cell and bulk levels. We found that cluster C1 significantly increased the expression of inflammatory factors, including IL-1 and IL-6, and the expression of chemokines, including CCL5 and CCL8, and decreased the expression of growth regulators such as IGFBP4. The activity of IL-1 links innate and adaptive immunity and can therefore be clinically translated into the context of preventive and therapeutic strategies by promoting T cell immunity [68]. Similarly, CCL5 and CCL8 were associated with T cell infiltration and response to ICB [69, 70]. The abnormal expression of these regulators in tumor tissues presumably determines the difference in both prognosis and response to ICB between patients in clusters C1 and C2.

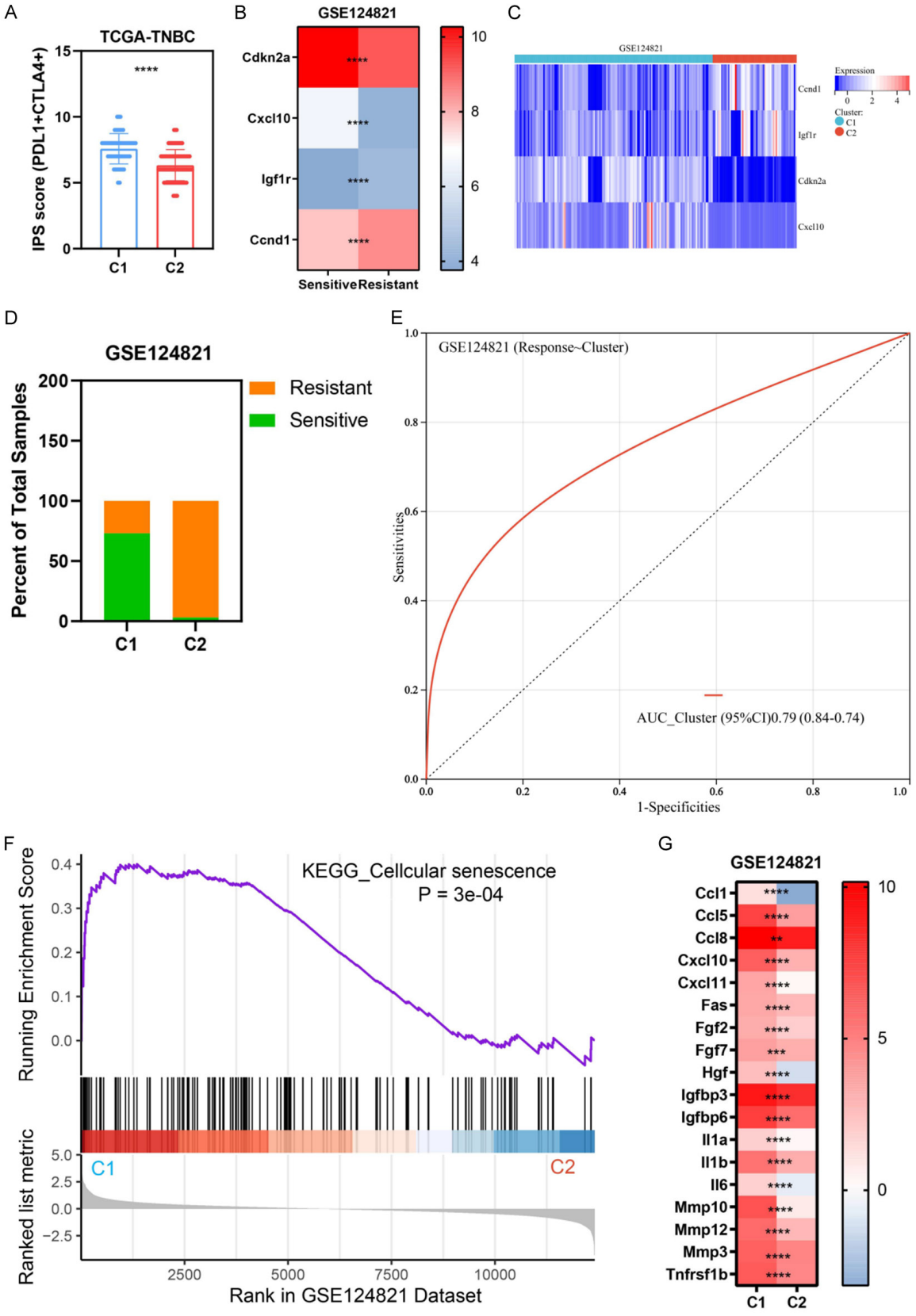

Figure 9. Identification of C1 cluster as the subtype with well response to ICB. A. The bar plot showed samples in C1 cluster had higher immunophenoscores (IPS) than that in C2 cluster using data from the TCGA-TNBC. B. The heatmap plot showed that samples sensitive to immune checkpoint blockade (ICB) had a higher expression of Cdkn2a,

Cxcl10 and a lower expression of Ccnd1, Igf1r than samples resistant to ICB in the GSE124821 dataset. C. The heatmap plot exhibited the expressions of Cdkn2a, Cxcl10, Ccnd1, and Igf1r between C1 and C2 using data from the GSE124821 dataset. D. The bar plot showed C1 cluster had a higher percent of samples sensitive to ICB than C2 cluster. E. The receiver operating characteristic curve plot showed an area under curve value equal to 0.79 (95% CI: 0.84-0.74), which meant a great performance in predicting immune checkpoint blockade response. F. Gene Set Enrichment Analysis plot showed cellular senescence pathway was enriched in C1 cluster using data from the GSE124821 dataset. G. The heatmap plot exhibited that the transcriptomics expression levels of some senescence-associated secretory phenotype factors, such as Ccl1, Ccl5, Ccl8, Il1a, Il1b, Il6, Mmp3, Mmp10, Mmp12, Tnfrsf1b etc., was higher in C1 cluster than that in C2 cluster using data from the GSE124821 dataset. IPS, immunophenoscores; TNBC, triple-negative breast cancer; ICB, immune checkpoint blockade.

However, our study has some limitations. First, data of all patients with BC in the GSE75688 cohort were analyzed regardless of molecular subtype owing to a limited number of samples and single tumor cells. Second, although we performed a multi-immunohistochemistry assay in human TNBC specimens and found the expression of CDKN2A and CXCL10 to be positively associated with CD3 and CD8, the underlying molecular mechanism remains unclear and needs further investigation.

Conclusion

As the subtype-specific vulnerabilities of ICB in TNBC are unclear, we aimed to identify markers related to cellular senescence that could potentially serve as predictors of ICB response in TNBC. Here, we succeeded in developing a robust cellular senescence-related classifier of TNBC based on the expression of *CDKN2A*, *CXCL10*, *CCND1*, and *IGF1R* by analyzing data at both single-cell and bulk levels. The expression of these genes was found to be relevant to clinical outcomes and response to ICB across multiple cohorts.

Acknowledgements

Informed consent was obtained from all subjects involved in the study.

Disclosure of conflict of interest

None.

Abbreviations

TNBC, Triple negative breast cancer; ICB, Immune checkpoint blockade; SASP, Senescence-associated secretory phenotype; UAMP, Uniform manifold approximation and projection; DEGs, Differentially expressed genes; pCR, pathological complete remission; NMF, Non-negative matrix factorization; IPS, Immunophenoscores.

Address correspondence to: Tianhao Zhou, Department of Medical Oncology, Shanghai First People's Hospital, Shanghai Jiao Tong University School of Medicine, Shanghai 200080, China. E-mail: zhouth23@163.com; Xiaomin Li, Department of Radiology, Shanghai Ninth People's Hospital, Shanghai Jiao Tong University School of Medicine, Shanghai, China. E-mail: lxm549496172@163.com

References

[1] Robert C, Schachter J, Long GV, Arance A, Grob JJ, Mortier L, Daud A, Carlino MS, McNeil C, Lotem M, Larkin J, Lorigan P, Neyns B, Blank CU, Hamid O, Mateus C, Shapira-Frommer R, Kosh M, Zhou H, Ibrahim N, Ebbinghaus S and Ribas A. Pembrolizumab versus ipilimumab in advanced melanoma. N Engl J Med 2015; 372: 2521-2532.

[2] Chung HC, Piha-Paul SA, Lopez-Martin J, Schellens JHM, Kao S, Miller WH Jr, Delord JP, Gao B, Planchard D, Gottfried M, Zer A, Jalal SI, Penel N, Mehnert JM, Matos I, Bennouna J, Kim DW, Xu L, Krishnan S, Norwood K and Ott PA. Pembrolizumab after two or more lines of previous therapy in patients with recurrent or metastatic SCLC: results from the KEYNOTE-028 and KEYNOTE-158 studies. J Thorac Oncol 2020; 15: 618-627.

[3] Sharma P, Siddiqui BA, Anandhan S, Yadav SS, Subudhi SK, Gao J, Goswami S and Allison JP. The next decade of immune checkpoint therapy. Cancer Discov 2021; 11: 838-857.

[4] Senan S, Okamoto I, Lee GW, Chen Y, Niho S, Mak G, Yao W, Shire N, Jiang H and Cho BC. Design and rationale for a phase III, randomized, placebo-controlled trial of durvalumab with or without tremelimumab after concurrent chemoradiotherapy for patients with limited-stage small-cell lung cancer: the ADRIATIC study. Clin Lung Cancer 2020; 21: e84-e88.

[5] Ready N, Farago AF, de Braud F, Atmaca A, Hellmann MD, Schneider JG, Spigel DR, Moreno V, Chau I, Hann CL, Eder JP, Steele NL, Pieters A, Fairchild J and Antonia SJ. Third-line nivolumab monotherapy in recurrent SCLC: CheckMate 032. J Thorac Oncol 2019; 14: 237-244.

[6] Schmid P, Adams S, Rugo HS, Schneeweiss A, Barrios CH, Iwata H, Diéras V, Hegg R, Im SA, Shaw Wright G, Henschel V, Molinero L, Chui SY, Funke R, Husain A, Winer EP, Loi S and Emens LA. Atezolizumab and nab-paclitaxel in advanced triple-negative breast cancer. N Engl J Med 2018; 379: 2108-2121.

[7] Loibl S, Untch M, Burchardi N, Huober J, Sinn BV, Blohmer JU, Grischke EM, Furlanetto J, Tesch H, Hanusch C, Engels K, Rezai M, Jackisch C, Schmitt WD, von Minckwitz G, Thomalla J, Kümmel S, Rautenberg B, Fasching PA, Weber K, Rhiem K, Denkert C and Schneeweiss A. A randomised phase II study investigating durvalumab in addition to an anthracycline taxane-based neoadjuvant therapy in early triple-negative breast cancer: clinical results and biomarker analysis of GeparNuevo study. Ann Oncol 2019; 30: 1279-1288.

[8] Safonov A, Jiang T, Bianchini G, Győrffy B, Karn T, Hatzis C and Pusztai L. Immune gene expression is associated with genomic aberrations in breast cancer. Cancer Res 2017; 77: 3317-3324.

[9] Thomas A, Routh ED, Pullikuth A, Jin G, Su J, Chou JW, Hoadley KA, Print C, Knowlton N, Black MA, Demaria S, Wang E, Bedognetti D, Jones WD, Mehta GA, Gatza ML, Perou CM, Page DB, Triozzi P and Miller LD. Tumor mutational burden is a determinant of immune-mediated survival in breast cancer. Oncoimmunology 2018; 7: e1490854.

[10] He S and Sharpless NE. Senescence in health and disease. Cell 2017; 169: 1000-1011.

[11] Hanahan D. Hallmarks of cancer: new dimensions. Cancer Discov 2022; 12: 31-46.

[12] Xue W, Zender L, Miething C, Dickins RA, Hernando E, Krizhanovsky V, Cordon-Cardo C and Lowe SW. Senescence and tumour clearance is triggered by p53 restoration in murine liver carcinomas. Nature 2007; 445: 656-660.

[13] Wang B, Kohli J and Demaria M. Senescent cells in cancer therapy: friends or foes? Trends Cancer 2020; 6: 838-857.

[14] Cuollo L, Antonangeli F, Santoni A and Soriani A. The senescence-associated secretory phenotype (SASP) in the challenging future of cancer therapy and age-related diseases. Biology (Basel) 2020; 9: 485.

[15] Ruscetti M, Morris JP, Mezzadra R, Russell J, Leibold J, Romesser PB, Simon J, Kulick A, Ho YJ, Fennell M, Li J, Norgard RJ, Wilkinson JE, Alonso-Curbelo D, Sridharan R, Heller DA, de Stanchina E, Stanger BZ, Sherr CJ and Lowe SW. Senescence-induced vascular remodeling creates therapeutic vulnerabilities in pancreas cancer. Cell 2020; 181: 424-441, e421.

[16] Jerby-Arnon L, Shah P, Cuoco MS, Rodman C, Su MJ, Melms JC, Leeson R, Kanodia A, Mei S, Lin JR, Wang S, Rabasha B, Liu D, Zhang G, Margolais C, Ashenberg O, Ott PA, Buchbinder EI, Haq R, Hodi FS, Boland GM, Sullivan RJ, Frederick DT, Miao B, Moll T, Flaherty KT, Herlyn M, Jenkins RW, Thummalapalli R, Kowalczyk MS, Cañadas I, Schilling B, Cartwright ANR, Luoma AM, Malu S, Hwu P, Bernatchez C, Forget MA, Barbie DA, Shalek AK, Tirosh I, Sorger PK, Wucherpfennig K, Van Allen EM, Schadendorf D, Johnson BE, Rotem A, Rozenblatt-Rosen O, Garraway LA, Yoon CH, Izar B and Regev A. A cancer cell program promotes T cell exclusion and resistance to checkpoint blockade. Cell 2018; 175: 984-997, e24.

[17] Uceda-Castro R, Margarido AS, Cornet L, Vegna S, Hahn K, Song JY, Putavet DA, van Geldorp M, Çitirikkaya CH, de Keizer PLJ, Ter Beek LC, Borst GR, Akkari L, van Tellingen O, Broekman MLD, Vennin C and van Rheenen J. Re-purposing the pro-senescence properties of doxorubicin to introduce immunotherapy in breast cancer brain metastasis. Cell Rep Med 2022; 3: 100821.

[18] Bassez A, Vos H, Van Dyck L, Floris G, Arijs I, Desmedt C, Boeckx B, Vanden Bempt M, Nevelsteen I, Lambein K, Punie K, Neven P, Garg AD, Wildiers H, Qian J, Smeets A and Lambrechts D. A single-cell map of intratumoral changes during anti-PD1 treatment of patients with breast cancer. Nat Med 2021; 27: 820-832.

[19] Pusztai L, Yau C, Wolf DM, Han HS, Du L, Wallace AM, String-Reasor E, Boughey JC, Chien AJ, Elias AD, Beckwith H, Nanda R, Albain KS, Clark AS, Kemmer K, Kalinsky K, Isaacs C, Thomas A, Shatsky R, Helsten TL, Forero-Torres A, Liu MC, Brown-Swigart L, Petricoin EF, Wulfkuhle JD, Asare SM, Wilson A, Singhrao R, Sit L, Hirst GL, Berry S, Sanil A, Asare AL, Matthews JB, Perlmutter J, Melisko M, Rugo HS, Schwab RB, Symmans WF, Yee D, Van't Veer LJ, Hylton NM, DeMichele AM, Berry DA and Esserman LJ. Durvalumab with olaparib and paclitaxel for high-risk HER2-negative stage II/III breast cancer: results from the adaptively randomized I-SPY2 trial. Cancer Cell 2021; 39: 989-998, e5.

[20] Hollern DP, Xu N, Thennavan A, Glodowski C, Garcia-Recio S, Mott KR, He X, Garay JP, Carey-Ewend K, Marron D, Ford J, Liu S, Vick SC, Martin M, Parker JS, Vincent BG, Serody JS and Perou CM. B cells and T follicular helper cells mediate response to checkpoint inhibitors in high mutation burden mouse models of breast cancer. Cell 2019; 179: 1191-1206, e21.

[21] Goldman MJ, Craft B, Hastie M, Repečka K, McDade F, Kamath A, Banerjee A, Luo Y, Rogers D, Brooks AN, Zhu J and Haussler D. Visualizing and interpreting cancer genomics data

via the Xena platform. Nat Biotechnol 2020; 38: 675-678.
[22] Gao J, Aksoy BA, Dogrusoz U, Dresdner G, Gross B, Sumer SO, Sun Y, Jacobsen A, Sinha R, Larsson E, Cerami E, Sander C and Schultz N. Integrative analysis of complex cancer genomics and clinical profiles using the cBioPortal. Sci Signal 2013; 6: pl1.
[23] Curtis C, Shah SP, Chin SF, Turashvili G, Rueda OM, Dunning MJ, Speed D, Lynch AG, Samarajiwa S, Yuan Y, Gräf S, Ha G, Haffari G, Bashashati A, Russell R, McKinney S, Langerød A, Green A, Provenzano E, Wishart G, Pinder S, Watson P, Markowetz F, Murphy L, Ellis I, Purushotham A, Børresen-Dale AL, Brenton JD, Tavaré S, Caldas C and Aparicio S. The genomic and transcriptomic architecture of 2,000 breast tumours reveals novel subgroups. Nature 2012; 486: 346-352.
[24] Cerami E, Gao J, Dogrusoz U, Gross BE, Sumer SO, Aksoy BA, Jacobsen A, Byrne CJ, Heuer ML, Larsson E, Antipin Y, Reva B, Goldberg AP, Sander C and Schultz N. The cBio cancer genomics portal: an open platform for exploring multidimensional cancer genomics data. Cancer Discov 2012; 2: 401-404.
[25] Jézéquel P, Loussouarn D, Guérin-Charbonnel C, Campion L, Vanier A, Gouraud W, Lasla H, Guette C, Valo I, Verrièle V and Campone M. Gene-expression molecular subtyping of triple-negative breast cancer tumours: importance of immune response. Breast Cancer Res 2015; 17: 43.
[26] Chung W, Eum HH, Lee HO, Lee KM, Lee HB, Kim KT, Ryu HS, Kim S, Lee JE, Park YH, Kan Z, Han W and Park WY. Single-cell RNA-seq enables comprehensive tumour and immune cell profiling in primary breast cancer. Nat Commun 2017; 8: 15081.
[27] Wu SZ, Al-Eryani G, Roden DL, Junankar S, Harvey K, Andersson A, Thennavan A, Wang C, Torpy JR, Bartonicek N, Wang T, Larsson L, Kaczorowski D, Weisenfeld NI, Uytingco CR, Chew JG, Bent ZW, Chan CL, Gnanasambandapillai V, Dutertre CA, Gluch L, Hui MN, Beith J, Parker A, Robbins E, Segara D, Cooper C, Mak C, Chan B, Warrier S, Ginhoux F, Millar E, Powell JE, Williams SR, Liu XS, O'Toole S, Lim E, Lundeberg J, Perou CM and Swarbrick A. A single-cell and spatially resolved atlas of human breast cancers. Nat Genet 2021; 53: 1334-1347.
[28] Krug K, Jaehnig EJ, Satpathy S, Blumenberg L, Karpova A, Anurag M, Miles G, Mertins P, Geffen Y, Tang LC, Heiman DI, Cao S, Maruvka YE, Lei JT, Huang C, Kothadia RB, Colaprico A, Birger C, Wang J, Dou Y, Wen B, Shi Z, Liao Y, Wiznerowicz M, Wyczalkowski MA, Chen XS, Kennedy JJ, Paulovich AG, Thiagarajan M, Kinsinger CR, Hiltke T, Boja ES, Mesri M, Robles AI, Rodriguez H, Westbrook TF, Ding L, Getz G, Clauser KR, Fenyö D, Ruggles KV, Zhang B, Mani DR, Carr SA, Ellis MJ and Gillette MA. Proteogenomic landscape of breast cancer tumorigenesis and targeted therapy. Cell 2020; 183: 1436.
[29] Mertins P, Mani DR, Ruggles KV, Gillette MA, Clauser KR, Wang P, Wang X, Qiao JW, Cao S, Petralia F, Kawaler E, Mundt F, Krug K, Tu Z, Lei JT, Gatza ML, Wilkerson M, Perou CM, Yellapantula V, Huang KI, Lin C, McLellan MD, Yan P, Davies SR, Townsend RR, Skates SJ, Wang J, Zhang B, Kinsinger CR, Mesri M, Rodriguez H, Ding L, Paulovich AG, Fenyö D, Ellis MJ and Carr SA. Proteogenomics connects somatic mutations to signalling in breast cancer. Nature 2016; 534: 55-62.
[30] Butler A, Hoffman P, Smibert P, Papalexi E and Satija R. Integrating single-cell transcriptomic data across different conditions, technologies, and species. Nat Biotechnol 2018; 36: 411-420.
[31] Becht E, McInnes L, Healy J, Dutertre CA, Kwok IWH, Ng LG, Ginhoux F and Newell EW. Dimensionality reduction for visualizing single-cell data using UMAP. Nat Biotechnol 2019; 37: 38-44.
[32] Korsunsky I, Millard N, Fan J, Slowikowski K, Zhang F, Wei K, Baglaenko Y, Brenner M, Loh PR and Raychaudhuri S. Fast, sensitive and accurate integration of single-cell data with Harmony. Nat Methods 2019; 16: 1289-1296.
[33] Andreatta M and Carmona SJ. UCell: robust and scalable single-cell gene signature scoring. Comput Struct Biotechnol J 2021; 19: 3796-3798.
[34] Ritchie ME, Phipson B, Wu D, Hu Y, Law CW, Shi W and Smyth GK. limma powers differential expression analyses for RNA-sequencing and microarray studies. Nucleic Acids Res 2015; 43: e47.
[35] Zhou Y, Zhou B, Pache L, Chang M, Khodabakhshi AH, Tanaseichuk O, Benner C and Chanda SK. Metascape provides a biologist-oriented resource for the analysis of systems-level datasets. Nat Commun 2019; 10: 1523.
[36] Cardoso AL, Fernandes A, Aguilar-Pimentel JA, de Angelis MH, Guedes JR, Brito MA, Ortolano S, Pani G, Athanasopoulou S, Gonos ES, Schosserer M, Grillari J, Peterson P, Tuna BG, Dogan S, Meyer A, van Os R and Trendelenburg AU. Towards frailty biomarkers: candidates from genes and pathways regulated in aging and age-related diseases. Ageing Res Rev 2018; 47: 214-277.
[37] Lee DD and Seung HS. Learning the parts of objects by non-negative matrix factorization. Nature 1999; 401: 788-791.

[38] Zeng D, Ye Z, Shen R, Yu G, Wu J, Xiong Y, Zhou R, Qiu W, Huang N, Sun L, Li X, Bin J, Liao Y, Shi M and Liao W. IOBR: multi-omics immuno-oncology biological research to decode tumor microenvironment and signatures. Front Immunol 2021; 12: 687975.
[39] Newman AM, Liu CL, Green MR, Gentles AJ, Feng W, Xu Y, Hoang CD, Diehn M and Alizadeh AA. Robust enumeration of cell subsets from tissue expression profiles. Nat Methods 2015; 12: 453-457.
[40] Yoshihara K, Shahmoradgoli M, Martínez E, Vegesna R, Kim H, Torres-Garcia W, Treviño V, Shen H, Laird PW, Levine DA, Carter SL, Getz G, Stemke-Hale K, Mills GB and Verhaak RGW. Inferring tumour purity and stromal and immune cell admixture from expression data. Nat Commun 2013; 4: 2612.
[41] Aran D, Hu Z and Butte AJ. xCell: digitally portraying the tissue cellular heterogeneity landscape. Genome Biol 2017; 18: 220.
[42] Becht E, Giraldo NA, Lacroix L, Buttard B, Elarouci N, Petitprez F, Selves J, Laurent-Puig P, Sautès-Fridman C, Fridman WH and de Reyniès A. Estimating the population abundance of tissue-infiltrating immune and stromal cell populations using gene expression. Genome Biol 2016; 17: 218.
[43] Finotello F, Mayer C, Plattner C, Laschober G, Rieder D, Hackl H, Krogsdam A, Loncova Z, Posch W, Wilflingseder D, Sopper S, Ijsselsteijn M, Brouwer TP, Johnson D, Xu Y, Wang Y, Sanders ME, Estrada MV, Ericsson-Gonzalez P, Charoentong P, Balko J, de Miranda NFDCC and Trajanoski Z. Molecular and pharmacological modulators of the tumor immune contexture revealed by deconvolution of RNA-seq data. Genome Med 2019; 11: 34.
[44] Li B, Liu JS and Liu XS. Revisit linear regression-based deconvolution methods for tumor gene expression data. Genome Biol 2017; 18: 127.
[45] Subramanian A, Tamayo P, Mootha VK, Mukherjee S, Ebert BL, Gillette MA, Paulovich A, Pomeroy SL, Golub TR, Lander ES and Mesirov JP. Gene set enrichment analysis: a knowledge-based approach for interpreting genome-wide expression profiles. Proc Natl Acad Sci U S A 2005; 102: 15545-15550.
[46] Hugo W, Zaretsky JM, Sun L, Song C, Moreno BH, Hu-Lieskovan S, Berent-Maoz B, Pang J, Chmielowski B, Cherry G, Seja E, Lomeli S, Kong X, Kelley MC, Sosman JA, Johnson DB, Ribas A and Lo RS. Genomic and transcriptomic features of response to anti-PD-1 therapy in metastatic melanoma. Cell 2016; 165: 35-44.
[47] Van Allen EM, Miao D, Schilling B, Shukla SA, Blank C, Zimmer L, Sucker A, Hillen U, Foppen MHG, Goldinger SM, Utikal J, Hassel JC, Weide B, Kaehler KC, Loquai C, Mohr P, Gutzmer R, Dummer R, Gabriel S, Wu CJ, Schadendorf D and Garraway LA. Genomic correlates of response to CTLA-4 blockade in metastatic melanoma. Science 2015; 350: 207-211.
[48] Bankhead P, Loughrey MB, Fernández JA, Dombrowski Y, McArt DG, Dunne PD, McQuaid S, Gray RT, Murray LJ, Coleman HG, James JA, Salto-Tellez M and Hamilton PW. QuPath: open source software for digital pathology image analysis. Sci Rep 2017; 7: 16878.
[49] Jackson JG, Pant V, Li Q, Chang LL, Quintás-Cardama A, Garza D, Tavana O, Yang P, Manshouri T, Li Y, El-Naggar AK and Lozano G. p53-mediated senescence impairs the apoptotic response to chemotherapy and clinical outcome in breast cancer. Cancer Cell 2012; 21: 793-806.
[50] Kang C, Xu Q, Martin TD, Li MZ, Demaria M, Aron L, Lu T, Yankner BA, Campisi J and Elledge SJ. The DNA damage response induces inflammation and senescence by inhibiting autophagy of GATA4. Science 2015; 349: aaa5612.
[51] Faust HJ, Zhang H, Han J, Wolf MT, Jeon OH, Sadtler K, Peña AN, Chung L, Maestas DR, Tam AJ, Pardoll DM, Campisi J, Housseau F, Zhou D, Bingham CO and Elisseeff JH. IL-17 and immunologically induced senescence regulate response to injury in osteoarthritis. J Clin Invest 2020; 130: 5493-5507.
[52] De Biasi S, Meschiari M, Gibellini L, Bellinazzi C, Borella R, Fidanza L, Gozzi L, Iannone A, Lo Tartaro D, Mattioli M, Paolini A, Menozzi M, Milić J, Franceschi G, Fantini R, Tonelli R, Sita M, Sarti M, Trenti T, Brugioni L, Cicchetti L, Facchinetti F, Pietrangelo A, Clini E, Girardis M, Guaraldi G, Mussini C and Cossarizza A. Marked T cell activation, senescence, exhaustion and skewing towards TH17 in patients with COVID-19 pneumonia. Nat Commun 2020; 11: 3434.
[53] Acosta JC, O'Loghlen A, Banito A, Guijarro MV, Augert A, Raguz S, Fumagalli M, Da Costa M, Brown C, Popov N, Takatsu Y, Melamed J, d'Adda di Fagagna F, Bernard D, Hernando E and Gil J. Chemokine signaling via the CXCR2 receptor reinforces senescence. Cell 2008; 133: 1006-1018.
[54] Taniguchi K and Karin M. NF-κB, inflammation, immunity and cancer: coming of age. Nat Rev Immunol 2018; 18: 309-324.
[55] Ladomersky E, Zhai L, Lauing KL, Bell A, Xu J, Kocherginsky M, Zhang B, Wu JD, Podojil JR, Platanias LC, Mochizuki AY, Prins RM, Kumthekar P, Raizer JJ, Dixit K, Lukas RV, Horbinski C, Wei M, Zhou C, Pawelec G, Campisi J, Grohmann U, Prendergast GC, Munn DH and Wainwright DA. Advanced age increases immunosuppression in the brain and decreas-

es immunotherapeutic efficacy in subjects with glioblastoma. Clin Cancer Res 2020; 26: 5232-5245.
[56] Brenner E, Schörg BF, Ahmetlić F, Wieder T, Hilke FJ, Simon N, Schroeder C, Demidov G, Riedel T, Fehrenbacher B, Schaller M, Forschner A, Eigentler T, Niessner H, Sinnberg T, Böhm KS, Hömberg N, Braumüller H, Dauch D, Zwirner S, Zender L, Sonanini D, Geishauser A, Bauer J, Eichner M, Jarick KJ, Beilhack A, Biskup S, Döcker D, Schadendorf D, Quintanilla-Martinez L, Pichler BJ, Kneilling M, Mocikat R and Röcken M. Cancer immune control needs senescence induction by interferon-dependent cell cycle regulator pathways in tumours. Nat Commun 2020; 11: 1335.
[57] Homann L, Rentschler M, Brenner E, Böhm K, Röcken M and Wieder T. IFN-γ and TNF induce senescence and a distinct senescence-associated secretory phenotype in melanoma. Cells 2022; 11: 1514.
[58] Burton DGA and Stolzing A. Cellular senescence: immunosurveillance and future immunotherapy. Ageing Res Rev 2018; 43: 17-25.
[59] Lin W, Wang X, Wang Z, Shao F, Yang Y, Cao Z, Feng X, Gao Y and He J. Comprehensive analysis uncovers prognostic and immunogenic characteristics of cellular senescence for lung adenocarcinoma. Front Cell Dev Biol 2021; 9: 780461.
[60] Peurala E, Koivunen P, Haapasaari KM, Bloigu R and Jukkola-Vuorinen A. The prognostic significance and value of cyclin D1, CDK4 and p16 in human breast cancer. Breast Cancer Res 2013; 15: R5.
[61] Ni J, Kabraji S, Xie S, Wang Y, Pan P, He X, Liu Z, Leone JP, Long HW, Brown MA, Winer EP, Dillon DAR, Lin NU and Zhao JJ. p16-deficiency predicts response to combined HER2 and CDK4/6 inhibition in HER2+ breast cancer brain metastases. Nat Commun 2022; 13: 1473.
[62] Arima Y, Hayashi N, Hayashi H, Sasaki M, Kai K, Sugihara E, Abe E, Yoshida A, Mikami S, Nakamura S and Saya H. Loss of p16 expression is associated with the stem cell characteristics of surface markers and therapeutic resistance in estrogen receptor-negative breast cancer. Int J Cancer 2012; 130: 2568-2579.
[63] Bostner J, Ahnström Waltersson M, Fornander T, Skoog L, Nordenskjöld B and Stål O. Amplification of CCND1 and PAK1 as predictors of recurrence and tamoxifen resistance in postmenopausal breast cancer. Oncogene 2007; 26: 6997-7005.
[64] Tobin NP, Sims AH, Lundgren KL, Lehn S and Landberg G. Cyclin D1, Id1 and EMT in breast cancer. BMC Cancer 2011; 11: 417.
[65] Aleksakhina SN, Kramchaninov MM, Mikushina AD, Kubrina SE, Petkau VV, Ivantsov AO, Moiseyenko VM, Imyanitov EN and Iyevleva AG. CCND1 and FGFR1 gene amplifications are associated with reduced benefit from aromatase inhibitors in metastatic breast cancer. Clin Transl Oncol 2021; 23: 874-881.
[66] Rigiracciolo DC, Nohata N, Lappano R, Cirillo F, Talia M, Scordamaglia D, Gutkind JS and Maggiolini M. IGF-1/IGF-1R/FAK/YAP transduction signaling prompts growth effects in triple-negative breast cancer (TNBC) cells. Cells 2020; 9: 1010.
[67] Wu Q, Tian AL, Li B, Leduc M, Forveille S, Hamley P, Galloway W, Xie W, Liu P, Zhao L, Zhang S, Hui P, Madeo F, Tu Y, Kepp O and Kroemer G. IGF1 receptor inhibition amplifies the effects of cancer drugs by autophagy and immune-dependent mechanisms. J Immunother Cancer 2021; 9: e002722.
[68] Van Den Eeckhout B, Tavernier J and Gerlo S. Interleukin-1 as innate mediator of T cell immunity. Front Immunol 2020; 11: 621931.
[69] Dangaj D, Bruand M, Grimm AJ, Ronet C, Barras D, Duttagupta PA, Lanitis E, Duraiswamy J, Tanyi JL, Benencia F, Conejo-Garcia J, Ramay HR, Montone KT, Powell DJ, Gimotty PA, Facciabene A, Jackson DG, Weber JS, Rodig SJ, Hodi SF, Kandalaft LE, Irving M, Zhang L, Foukas P, Rusakiewicz S, Delorenzi M and Coukos G. Cooperation between constitutive and inducible chemokines enables T cell engraftment and immune attack in solid tumors. Cancer Cell 2019; 35: 6.
[70] Sen T, Rodriguez BL, Chen L, Corte CMD, Morikawa N, Fujimoto J, Cristea S, Nguyen T, Diao L, Li L, Fan Y, Yang Y, Wang J, Glisson BS, Wistuba II, Sage J, Heymach JV, Gibbons DL and Byers LA. Targeting DNA damage response promotes antitumor immunity through STING-mediated T-cell activation in small cell lung cancer. Cancer Discov 2019; 9: 646-661.

Table S1. List of senescence related genes

	KEGG	GO	Frailty biomarkers*
	hsa04218	GO:0090398	Core panel
hsa04218	TGFB1	TERF2	IL6
TGFB1	TGFB2	CDK2	CXCL10
TGFB2	TGFB3	MAPK10	CX3CL1
TGFB3	TGFBR1	BRCA2	GDF15
TGFBR1	TGFBR2	H2AFX	FNDC5
TGFBR2	SMAD2	MAPKAPK5	VIM
SMAD2	SMAD3	TP53	PLAU
SMAD3	CDKN2B	CDKN1B	AGT
CDKN2B	CDK4	ATM	BDNF
CDK4	CDK6	ARNTL	FGF23
CDK6	CCND1	SMC5	FGF21
CCND1	CCND2	NSMCE2	RGN
CCND2	CCND3	OPA1	CALR
CCND3	RB1	LMNA	AGRN
RB1	RBL1	MIF	GRN
RBL1	RBL2	TBX3	KL
RBL2	E2F1	PLA2R1	LEP
E2F1	E2F2	SMC6	AHCY
E2F2	E2F3	TBX2	KRT18
E2F3	E2F4	ULK3	
E2F4	E2F5	CDKN1A	
E2F5	PIK3CA	PML	
PIK3CA	PIK3CD	WNT16	
PIK3CD	PIK3CB	DNAJA3	
PIK3CB	PIK3R1	MAP2K6	
PIK3R1	PIK3R2	SIRT1	
PIK3R2	PIK3R3	HMGA1	
PIK3R3	FOXO1	CITED2	
FOXO1	FOXO3	IGF1R	
FOXO3	CDKN1A	KAT5	
CDKN1A	CDK2	PRELP	
CDK2	CCNE1	MAGEA2B	
CCNE1	CCNE2	KAT6A	
CCNE2	HLA-A	MAP3K5	
HLA-A	HLA-B	NPM1	
HLA-B	HLA-C	MAPK11	
HLA-C	HLA-F	ID2	
HLA-F	HLA-G	C2orf40	
HLA-G	HLA-E	PRMT6	
HLA-E	KIR2DL4	SPI1	
KIR2DL4	KRAS	MAPK14	
KRAS	NRAS	CDKN2B	
NRAS	RRAS	CDKN2A	
RRAS	RRAS2	HMGA2	
RRAS2	MRAS	CALR	
MRAS	HRAS	ABL1	

HRAS	AKT1	NUP62
AKT1	AKT2	TP63
AKT2	AKT3	ZMIZ1
AKT3	TSC1	MAP2K3
TSC1	TSC2	MAP2K4
TSC2	RHEB	MAPK9
RHEB	MTOR	MAPK8
MTOR	PTEN	WRN
PTEN	SIRT1	MAP2K7
SIRT1	CCNA2	SRF
CCNA2	CCNA1	MAP2K1
CCNA1	MYBL2	HRAS
MYBL2	LIN9	PRKCD
LIN9	LIN37	MNT
LIN37	LIN52	
LIN52	LIN54	
LIN54	RBBP4	
RBBP4	FOXM1	
FOXM1	MYC	
MYC	CDKN2A	
CDKN2A	MDM2	
MDM2	TP53	
TP53	RASSF5	
RASSF5	BTRC	
BTRC	FBXW11	
FBXW11	HIPK3	
HIPK3	HIPK1	
HIPK1	HIPK2	
HIPK2	HIPK4	
HIPK4	PPP1CA	
PPP1CA	PPP1CB	
PPP1CB	PPP1CC	
PPP1CC	RAF1	
RAF1	MAP2K1	
MAP2K1	MAP2K2	
MAP2K2	MAPK1	
MAPK1	MAPK3	
MAPK3	ETS1	
ETS1	MAP2K3	
MAP2K3	MAP2K6	
MAP2K6	MAPK11	
MAPK11	MAPK12	
MAPK12	MAPK13	
MAPK13	MAPK14	
MAPK14	GADD45A	
GADD45A	GADD45B	
GADD45B	GADD45G	
GADD45G	CDK1	
CDK1	CCNB1	

CCNB1	CCNB2
CCNB2	CCNB3
CCNB3	MRE11
MRE11	RAD50
RAD50	NBN
NBN	ATM
ATM	CHEK2
CHEK2	RAD9A
RAD9A	RAD9B
RAD9B	RAD1
RAD1	HUS1
HUS1	ATR
ATR	CHEK1
CHEK1	CDC25A
CDC25A	SQSTM1
SQSTM1	GATA4
GATA4	TRAF3IP2
TRAF3IP2	NFKB1
NFKB1	RELA
RELA	IL1A
IL1A	IL6
IL6	CXCL8
CXCL8	IGFBP3
IGFBP3	SERPINE1
EIF4EBP1	MAPKAPK2
MAPKAPK2	ZFP36L1
ZFP36L1	ZFP36L2
ZFP36L2	CACNA1D
CACNA1D	TRPV4
TRPV4	TRPM7
TRPM7	CAPN1
CAPN1	CAPN2
CAPN2	CALML3
CALML3	CALM2
CALM2	CALM3
CALM3	CALM1
CALM1	CALML6
CALML6	CALML5
CALML5	CALML4
CALML4	PPP3CA
PPP3CA	PPP3CB
PPP3CB	PPP3CC
PPP3CC	PPP3R1
PPP3R1	PPP3R2
PPP3R2	NFATC1
NFATC1	NFATC2
NFATC2	NFATC3
NFATC3	NFATC4
NFATC4	ITPR1

ITPR1	ITPR2
ITPR2	ITPR3
ITPR3	SLC25A4
SLC25A4	SLC25A5
SLC25A5	SLC25A6
SLC25A6	SLC25A31
SLC25A31	PPID
PPID	VDAC1
VDAC1	VDAC2
VDAC2	VDAC3
VDAC3	MCU
MCU	

*Refence (PMID: 30071357).

Table S2. The clinical information of patients and results of multiplex immunofluorescence assay

Patient	CXCL10	IGF1R	CD3	CD8	DAPI	CXCL10/ DAPI	IGF1R/ DAPI	CD3/ DAPI	CD8/ DAPI	age	Sex	Patho-logical diagnosis	Patho-logical grade	Tumor size stage	Lymphnode metastatic stage	TNM stage	ER	PR	HER2/ ERBB2	Mo-lecular subtype
P1	211	451	181	4	15429	0.013676	0.029231	0.011731	0.000259	44	Female	IDC	II	T2	N2	T2N2M0	-	-	-	TNBC
P2	76	195	1010	48	16500	0.004606	0.011818	0.061212	0.002909	37	Female	IDC	II	T1	N2	T1N2M0	-	-	-	TNBC
P3	3849	7113	1283	157	15769	0.244086	0.451075	0.081362	0.009956	37	Female	IDC	III	T1	N0	T1N0M0	-	-	-	TNBC
P4	3898	16	6114	3519	27035	0.144183	0.000592	0.226151	0.130165	47	Female	IDC	III	T1	N0	T1N0M0	-	-	-	TNBC
P5	1091	6083	1790	207	17669	0.061747	0.344275	0.101307	0.011715	66	Female	IDC	II	T2	N1	T2N1M0	-	-	-	TNBC
P6	5857	20	2766	566	12918	0.453398	0.001548	0.21412	0.043815	69	Female	IDC	II-III	T2	N2	T2N2M0	-	-	-	TNBC
P7	2783	5521	1642	513	19007	0.14642	0.290472	0.086389	0.02699	51	Female	IDC	II-III	T1	N0	T1N0M0	-	-	-	TNBC
P8	4600	5983	310	163	22366	0.205669	0.267504	0.01386	0.007288	48	Female	IDC	II-III	T1	N1	T1N1M0	-	-	-	TNBC
P9	2202	699	705	416	13452	0.163693	0.051963	0.052409	0.030925	52	Female	IDC	II-III	T2	N0	T2N0M0	-	-	-	TNBC
P10	4279	21	3554	1155	21003	0.203733	0.001	0.169214	0.054992	38	Female	IDC	II	T2	N0	T2N0M0	-	-	-	TNBC
P11	4501	370	1429	527	14484	0.310757	0.025545	0.098661	0.036385	48	Female	IDC	III	T2	N0	T2N0M0	-	-	-	TNBC
P12	4649	6973	819	353	15131	0.30725	0.460842	0.054127	0.02333	62	Female	IDC	III	T2	N0	T2N0M0	-	-	-	TNBC
P13	2945	274	476	176	19408	0.151742	0.014118	0.024526	0.009068	48	Female	IDC	III	T1	N0	T1N0M0	-	-	-	TNBC
P14	1931	5758	14	10	8687	0.222286	0.66283	0.001612	0.001151	42	Female	IDC	II	T4	N3	T4N3M0	-	-	-	TNBC
P15	1736	153	526	139	2572	0.674961	0.059487	0.20451	0.054044	45	Female	IDC	II	T2	N1	T2N1M0	-	-	-	TNBC
P16	513	4502	136	92	18513	0.02771	0.24318	0.007346	0.004969	39	Female	IDC	III	T2	N1	T2N1M0	-	-	-	TNBC
P17	9451	47	4795	463	15766	0.599455	0.002981	0.304135	0.029367	47	Female	IDC	III	T2	N0	T2N0M0	-	-	-	TNBC
P18	1065	8330	76	5	18635	0.057151	0.447008	0.004078	0.000268	64	Female	IDC	III	T2	N0	T2N0M0	-	-	-	TNBC